Influence of chloride-induced corrosion cracks on the strength of reinforced concrete

A thesis submitted to RMIT University
in fulfillment of the requirements for
the degree of Master of Civil Engineering

Denglei Tang B. Eng.

School of Civil, Environmental and Chemical Engineering

RMIT University

October 2007

Declaration

This is to certify that:

1. except where due acknowledgement has been made, the work is that of the candidate alone;
2. the work has not been submitted previously, in whole or in part, to qualify for any other academic award;
3. the content of the thesis is the result of work which has been carried out since the official commencement date of the approved research program;
4. any editorial work, paid or unpaid, carried out by a third party is acknowledged.

Signed: ……

Acknowledgement

I wish to express my sincere gratitude to my supervisor, Dr. Tom Molyneaux, who has given abundant support to my research work over the past two years. He has always been encouraging, patient and responsive. His advice has always been helpful which has given me a lot of inspiration in my research work. I have been really impressed by and have benefited from his guidance in engineering thinking, technical writing and personal assistance, which has enabled me to finish my project successfully. I also wish to express my gratitude to my consultant Dr. Dave Law, for his advice and guidance on this project. His comments and contribution to this project have been vital. In addition, I would also like to thank my second supervisor Dr. Rebecca Gravina for her support when I needed help.

I would also like to thank the technical staffs who help me during the two year's study. I wish to thank Mr. Ray Treacy and Mr. David Friedman for providing valuable suggestions and technical assistance in making the models and testing rigs.

I would like to thank my school for the scholarship support. It is in the excellent School of Civil and Chemical Engineering, RMIT University that my postgraduate research has been carried out. The School has provided me with high quality research resources and facilities and a positive study environment. I will never forget the research experience in RMIT University.

Finally, deep appreciation goes to my family in China: my parents. They gave me emotional and financial support during these years. And thanks to my fiancé who accompanied me and took care of me throughout the good times and bad times.

Table of Content

Declaration ii
Acknowledgement iii
Table of Content iv
List of figures v
List of tables vii
Notation viii
Abstract 1
1 Introduction 2
2 Background 3
2.1 Literature review 3
2.1.1 Theory of corrosion in reinforced concrete (RC) construction 3
2.1.2 Corrosion cracks 5
2.1.3 Bond behaviour 7
2.2 Preliminary investigations 10
3 Methodology 12
3.1 Design of specimens 12
3.1.1 General 12
3.1.2 Selection of test models 14
3.2 Testing procedure 15
3.2.1 Calibration of equipments 16
3.2.2 Accelerating corrosion 17
3.2.3 Pull-out system 18
4 Test results 20
4.1 Analysis of concrete compressive strength 20
4.2 Extent of corrosion 23
4.2.1 Assessment of extent of corrosion 23
4.2.2 Comparison of theoretical and actual mass loss 24
4.3 Bond strength of corroded reinforcement 27
4.3.1 Assessment of bond strength 27
4.3.2 Influence of testing sequence 27
4.3.3 Experimental results of bond strength with related cracks and corrosion extent. 27
4.4 Pit characteristics 32
4.5 Bond vs slip 39
4.6 Cracks pattern 45
5 Discussion 48
5.1 Effect of bar position 48
5.2 Bar size effects 48
5.3 Effect of concrete strength on bond strength 50
5.4 Effect of crack width and extent of corrosion on bond strength loss 51

5.5 Influence of C/Φ ratio 58
5.6 Extent of corrosion vs crack width 59
5.7 Effect of impressed current 61
5.8 Characteristics of corroded steel bars 62
5.8.1 Bond stress development length 62
5.8.2 Rupture of steel bars during pullout test 63
6 Conclusions and Recommendations 68
7 References 70
Appendix 74

List of figures

Figure 2.1 Electrolytic cell 3
Figure 2.2 Tafel ring 8
Figure 2.3 Effects of corrosion on residual strength 9
Figure 2.4 Variation in bond strength with corrosion (Schematic) 10
Figure 3.1 Compressive test Figure 3.2 Tensile strength test 13
Figure 3.3 Rib geometry of Grade 500 N steel reinforcing bars 13
Figure 3.4 RILEM concentric pullout specimen 14
Figure 3.5 Sketch of adopted beam end specimen 15
Figure 3.6 Calibration curve at loaded end LVDT 16
Figure 3.7 Calibration curve of free end LVDT 16
Figure 3.8 Calibration curve of load cell 17
Figure 3.9 Accelerating system 17
Figure 3.10 Pull-out test 19
Figure 3.11 Loading scheme 19
Figure 4.1 Compressive strength vs tensile strength 21
Figure 4.2 Comparison of theoretical mass loss and actual mass loss 25
Figure 4.3 Comparison of theoretical mass loss and actual mass loss 25
Figure 4.4 Comparison of theoretical mass loss and actual mass loss 26
Figure 4.5 Comparison of theoretical mass loss and actual mass loss 26
Figure 4.6 Splitting failure Figure 4.7 Splitting-induced pull-out Failure 27
Figure 4.8 Dial gauge for measuring pits depth 33
Figure 4.9 Non-corroded 16 mm bar 33
Figure 4.10 Corroded 16 mm bar with approximately 15% mass loss 33
Figure 4.11 Corroded 12 mm bar with approximately 5% mass loss 33

Figure 4.12 Corroded 12 mm bar with approximately 20% mass loss.....33
Figure 4.13 Corroded 12 mm bar with approximately 30% mass loss.....34
Figure 4.14 Bond strength vs average pits depth for 12 mm bars with 1 C/Φ.....35
Figure 4.15 Bond strength vs maximum pits depth for 12 mm bars with 1 C/Φ.....35
Figure 4.16 Bond strength vs section loss for 12 mm bars with 1 C/Φ.....35
Figure 4.17 Bond strength vs average pits depth for 12 mm bars with 3 C/Φ.....36
Figure 4.18 Bond strength vs maximum pits depth for 12 mm bars with 3 C/Φ.....36
Figure 4.19 Bond strength vs section loss for 12 mm bars with 3 C/Φ.....36
Figure 4.20 Bond strength vs average pits depth for 16 mm bars with 1 C/Φ.....37
Figure 4.21 Bond strength vs maximum pits depth for 16 mm bars with 1 C/Φ.....37
Figure 4.22 Bond strength vs section loss for 16 mm bars with 1 C/Φ.....37
Figure 4.23 Bond strength vs average pits depth for 16 mm bars with 3 C/Φ.....38
Figure 4.24 Bond strength vs maximum pits depth for 16 mm bars with 3 C/Φ.....38
Figure 4.25 Bond strength vs section loss for 16 mm bars with 3 C/Φ.....38
Figure 4.26 Main pit pattern (top view).....39
Figure 4.27 Peak bond force vs free end slip for 12 mm bars with 1 C/Φ with different extent of corrosion.....41
Figure 4.28 Peak bond force vs free end slip for 12 mm bars with 3 C/Φ with different extent of corrosion.....42
Figure 4.29 Peak bond force vs free end slip for 16 mm bars with 1 C/Φ with different extent of corrosion.....43
Figure 4.30 Peak bond force vs free end slip for 16 mm bars with 3 C/Φ with different extent of corrosion.....44
Figure 4.31 Type 1.....46
Figure 4.32 Type 2.....46
Figure 4.33 Type 3.....46
Figure 4.34 Type 4.....46
Figure 4.35 Type 5.....47
Figure 4.36 Type 6.....47
Figure 5.1 Bar size effect on specimens with the same C/Φ.....49
Figure 5.2 Peak bond strength vs average surface crack width for 12 mm bars with 1 C/Φ.....52
Figure 5.3 Peak bond strength vs maximum surface crack width for 12 mm bars with 1 C/Φ52
Figure 5.4 Peak bond strength vs extent of corrosion for 12 mm bars with 1 C/Φ.....53
Figure 5.5 Peak bond strength vs average surface crack width for 12 mm bars with 3 C/Φ.....54
Figure 5.6 Peak bond strength vs maximum surface crack width for 12 mm bars with 3 C/Φ54

Figure 5.7 Peak bond strength vs extent of corrosion for 12 mm bars with 3 C/Φ 55
Figure 5.8 Peak bond strength vs average surface crack width for 16 mm bars with 1 C/Φ ... 55
Figure 5.9 Peak bond strength vs maximum surface crack width for 16 mm bars with 1 C/Φ 56
Figure 5.10 Peak bond strength vs extent of corrosion for 16 mm bars with 1 C/Φ 56
Figure 5.11 Peak bond strength vs average surface crack width for 16 mm bars with 3 C/Φ . 57
Figure 5.12 Peak bond strength vs maximum surface crack width for 16 mm bars with 3 C/Φ 57
Figure 5.13 Peak bond strength vs extent of corrosion for 16 mm bars with 3 C/Φ 58
Figure 5.14 Crack width vs corrosion level for 12 mm bars 60
Figure 5.15 Crack width vs corrosion level for 16 mm bars 60
Figure 5.16 Peak bond force vs loaded end slip 64
Figure 5.17 Peak bond force vs free end slip 64
Figure 5.18 Peak bond force vs loaded end slip 65
Figure 5.19 Peak bond force vs free end slip 65
Figure 5.20 Peak bond force vs loaded end slip 65
Figure 5.21 Peak bond force vs free end slip 66
Figure 5.22 Combined effect of localized corrosion and 67

List of tables

Table 3.1 Material information 12
Table 3.2 Concrete mix design 12
Table 3.3 Specimen specifications 15
Table 4.1 Compressive strength for 40 MPa specimens 20
Table 4.2 Tensile strength for 40 MPa specimens 20
Table 4.3 50 MPa specimens 21
Table 4.4 Detailed information of cast concrete 22
Table 4.5 12 mm reinforcement with 1 C/Φ 29
Table 4.6 12 mm reinforcement with 3 C/Φ 30
Table 4.7 16 mm reinforcement with 1 C/Φ 31
Table 4.8 16 mm reinforcement with 3 C/Φ 32
Table 4.9 Summary of types of cracks pattern 47
Table 5.1 Bond strength of non-cracked specimens 49
Table 5.2 Normalised bond strength 51
Table 5.3 Results of specimens under accelerated and natural corrosion 62

Notation

Symbols used in this thesis are listed below.

A_b	= cross-sectional area of a reinforcing bar
ΔA_s	= steel loss of cross-section
ΔA_{s0}	= steel cross-section loss needed for cracking initiation
a	= distance
C	= concrete cover
F	= Faraday's constant
f_c	= experimental compressive strength
$f_{c,sp}$	= tensile strength
G	= final weight of the steel bar after removal of the corrosion products
G_0	= initial weight of the steel bar before corrosion
g_0	= weight per unit length of the steel bar
I	= current
I_{corr}	= corrosion current
k	= a coefficient, ratio, or factor used with and without numerical subscripts
M	= atomic weight of the metal
Δ m	= mass of steel consumed
T	= time of current flow
t	= time
W	= estimated crack width
x	= corrosion penetration
z	= ionic charge
α	= corrosion factor
β	= a coefficient which depends on the position of the bar in the section
τ'	= bond strength for grade 40 concrete
τ_{exptl}	= experimental bond strength
τ	= a bond strength
Φ	= bar diameter
Φ (t)	= bar diameter(mm) at time t
Φ(i)	= initial bar diameter

Abstract

In marine environments and where de-icing salts are applied, the degradation of reinforced concrete structures due to chloride induced corrosion of the reinforcement is a major problem. The expansive nature of the corrosion process results in cracking of the concrete and eventually spalling. In order to select suitable remedial measures it is necessary to make an assessment of the residual strength and the residual life.

In order to investigate the effect of corrosion on bond strength of the reinforcement, specimens comprising square prismatic sections containing steel reinforcement in the four corners have been subjected to a wet-dry cycle and corrosion has been accelerated by polarising the bars. The research has studied the change of bond strength with level of corrosion for 12 mm and 16 mm bars with concrete cover of 1 and 3 times the bar size. The bond strength is assessed by means of pull out tests and the corresponding extent of corrosion has been assessed in terms of the mass loss. Observations and measurements of the form of the corrosion (pit dimensions and loss of bar diameter) are also presented.

The relationship between bond strength and surface crack width has been investigated. Results show that the surface crack width may be a good indicator of residual bond strength. In addition, the influence on bond strength of concrete compressive strength, reinforcement cover, bar position and bar size on the change of bond strength has been explored.

It should be noted that all conclusions drawn in this project are based on tests on specimens without shear reinforcement (unconfined) and that accelerated corrosion (by impressed current) has been adopted. Consequently, care should be exercised in applying these results directly to structures in the field. Additional research is needed to assess the influence of impressed current on crack patterns and the effect of shear reinforcement.

1 Introduction

In reinforced concrete, it is the bond behaviour between the reinforcement and the concrete that ensures effective composite behaviour. However, reinforcement corrosion affects composite performance because the corrosion products formed around the steel bars ultimately result in a deterioration of the bond. The deterioration of structures due to the corrosion of the reinforcement is mainly characterized by a general or local section loss of the reinforcing bars, cracks in the concrete and loss of bond strength.

In order to assess the service life of reinforced concrete (RC) structures, a significant volume of previous research has been undertaken, focusing on the relationship between the corrosion level (corrosion penetration or mass loss of the steel) and cracks [1-8]; current density versus surface crack width [1, 2, 9]; and bond strength versus corrosion level (mass loss or corrosion penetration) [10-17]. Relatively little research has studied the relationship between bond strength and surface crack width [11, 13]. Consequently, the aim of this research has been to study the relationship between the change of bond strength and the surface crack width. Corrosion penetration has been examined and related to bar diameter. In addition, the theoretical steel mass loss based on Faraday's law has been assessed, along with bond slip characteristics.

Chapter 2 discusses the basic theory used through the project, Chapter 3 the methodology of the project and gives details of testing procedure, Chapter 4 presents the test results, Chapter 5 offers a discussion of the results and Chapter 6 summarises the conclusions and recommends future work.

2 Background

2.1 Literature review

2.1.1 Theory of corrosion in reinforced concrete (RC) construction

Corrosion of reinforced concrete is a complex electrochemical mechanism that occurs at the interface of the concrete and the steel bars. It involves chemical reactions (gain and loss of electrons) and electrical currents. In reinforced concrete, a passive oxide coating forms on the reinforcing bars due to the alkaline conditions (high pH, normally about 12.5) derived from reactions between the mix water and the Portland cement particles. This layer prevents the steel bars from corroding. However, if the passive coating on the steel is lost, due to carbonation or the presence of chloride ions (above a critical concentration), corrosion may begin. Heterogeneities in the surface of the steel allow it to function as a mixed electrode, allowing a region of the steel to act as an anode and another region to act as a cathode. The water in the pores of the cement paste contains various dissolved ions and serves as the electrolyte. At anodic sites, iron atoms pass into solution as ferrous ions (positively charged), free electrons flow through the same bar to the cathodic region where electrons are accepted. Thus, we have an electrolytic cell Figure 2.1 [18].

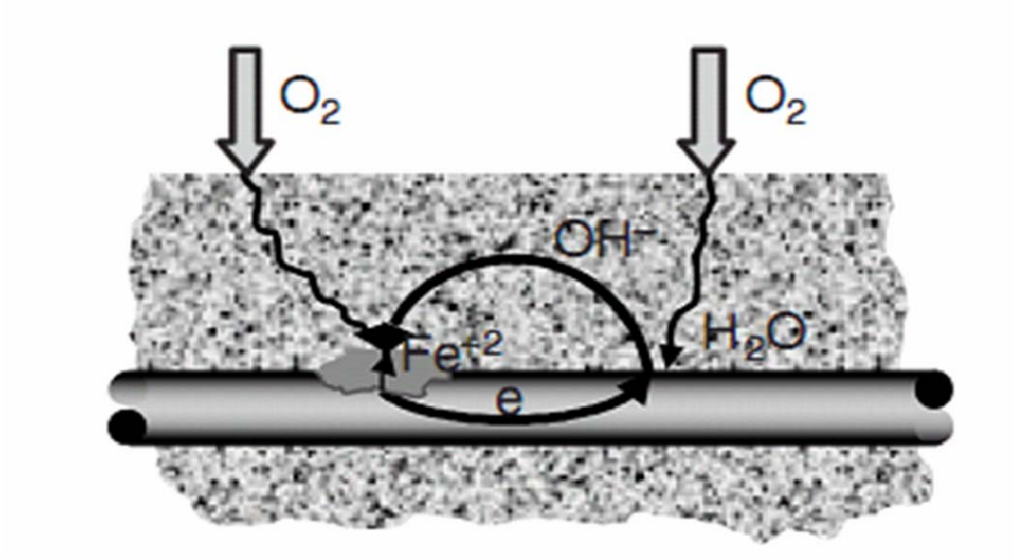

Figure 2.1 Electrolytic cell

Anodic reaction: $Fe \rightarrow Fe^{2+} + 2e^{-}$

Cathodic reaction: $O_2 + 2H_2O + 4e^{-} \rightarrow 4OH^{-}$

Other forms of rust: FeO, Fe_3O_4, Fe_2O_3, and $Fe(OH)_3$, are also formed depending on conditions. From the above simplified explanation, the following conditions for corrosion to

occur in RC are required:

- Loss of passivation
- Presence of moisture
- Presence of oxygen

Once the passive layer breaks down, rust appears on the surface of the bar. Because the volume of the corrosion products is greater than that of the steel consumed during the process of corrosion, radial and circumferential stresses are generated in the concrete around the steel bars, resulting in the cracking of the surrounding concrete.

The amount of steel lost due to corrosion can be calculated by applying Faraday's law [19]. This relates the corrosion current to the loss of steel mass by accounting for the charge on each ion that is transported during the process.

$$\Delta m = MIt / zF \qquad (2.1)$$

Where Δ m is the mass of steel consumed (gm), M is the atomic weight of the metal (56gm for iron); t is the time in seconds; z is the ionic charge (2 for iron); and F is Faraday's constant (96,500 amp.s)
The resulting equation in terms of penetration is:

$$x = 11.6 I_{corr} t \qquad (2.2)$$

Where x is the corrosion penetration in microns; t is the time in years elapsed since the onset of corrosion and I_{corr} is the corrosion current in μ A/cm^2 throughout time t.

The method of applying an impressed current to accelerate corrosion has been used by many researchers in order to obtain results in a reasonable time [1, 2, 5, 7-14, 16, 17, 20-27]. Table 2.1 shows the impressed current density used in different research work. Faraday's law may be used to determine the current required to achieve a pre-determined mass loss from the steel. Maximum corrosion rates measured on actual structures are generally less than 10 μA/cm^2. However, the maximum natural corrosion rate (without impressed current) reported from measurements taken in laboratory studies is approximately 100 μA/cm^2. The majority of previous studies using impressed currents have used current densities that are 3 to 100 times

greater than this [9]. The current density levels are known to affect the surface crack width, probably because a low current density level gives corrosion products more time to dissipate through the concrete pores [2, 9]. Research [9] suggests that current densities up to 200 μA/cm^2 result in similar stresses during the early stages of corrosion when compared to 100 μA/cm^2. Consequently, the work reported here has adopted a current density of 200 μA/cm^2, falling within the range of previous similar work whilst achieving the required extent of corrosion within a reasonable time (one month).

Author	Year	Impressed Current
Al-Sulaimani[23]	1990	2000 μA/cm^2
Rasheeduzzafar[24]	1992	3000 μA/cm^2
Rodriguze et al.[25]	1994	100 μA/cm^2
Gonzalez et al.[21]	1995	10~100 μA/cm^2
Andrade et al.[2]	1996	3~100 μA/cm^2
Cabrera[12]	1996	3 V
Almusallam et al.[13]	1996	0.4 A(3469 μA/cm^2)
Alonso et al.[1]	1998	100 μA/cm^2
Mangat et al.[26]	1999	800~2400 μA/cm^2
Stanish et al.[14]	1999	100 mA
Amleh et al[10]	1999	5 V
Auyeung et al.[27]	2000	12 A
Lee et al.[17]	2002	1 A (9663.8 μA/cm^2)
Maaddawy et al.[5, 9]	2003	100~500 μA/cm^2
	2005	215 mA
Vu et al.[7]	2005	100 μA/cm^2
Fang et al.[16]	2006	0~2 A (0~88464 μA/cm^2)

Table 2.1 Review of impressed current density used by others

2.1.2 Corrosion cracks

Surface cracking due to corrosion of RC structures has been investigated by other researchers [1, 3-6, 8, 11-13, 28-31]. When the production of rust begins, it gradually builds pressure around the reinforcing steel. This build up of pressure eventually cracks the concrete around the steel, and the crack or cracks propagate with further increase of pressure. If the cracks

propagate to the surface, the concrete will eventually begin breaking off or spalling. Andrade et al. [32] assessed cracking conditions in corroded structures. They proposed the following relationship between crack width and corrosion penetration:

$$W = 0.05 + \beta(x - x_0) \quad [W \leq 1.0 \text{ mm}] \qquad (2.3)$$

Where W is the estimated crack width (mm), x is the corrosion penetration (microns), x_0 is the corrosion penetration (microns) at crack initiation and β is a coefficient which depends on the position of the bar in the section (β=0.01 for top cast bars and 0.0125 for bottom cast bars). They suggested that the x_0 needed for the cracking initiation can be estimated by the following expression:

$$x_0 = 83.8 + 7.4c/\phi - 22.6 f_{c,sp} \qquad (2.4)$$

Where c is the concrete cover (mm); Φ is the bar diameter (mm), $f_{c,sp}$ is the tensile strength (MPa)

Alternatively Equation 2.5 is recommended by Alonso et al. [1] based on a study of the influence of the cover/diameter ratio:

$$x_0 = 7.53 + 9.32C/\Phi \qquad (2.5)$$

Where C is the concrete cover (mm); Φ is the bar diameter (mm). Previous work comparing these two approaches by Vidal et al. [3] concluded that their experimental results are more in agreement with the predictions calculated using Equation (2.5) than Equation (2.4). This is because the model predictions become erroneous (x_0<0) in Equation (2.4) when a concrete tensile strength equal to 4.1MPa (C/Φ=1). They proposed another Equation (2.6) to relate the cracks and steel loss of section.

$$W = k(\Delta A_s - \Delta A_{s0}) \qquad (2.6)$$

Where W is the crack width (mm); ΔA_s is the steel loss of cross-section in mm2; ΔA_{s0} is

the steel cross-section loss needed for cracking initiation; k=0.0575; $r^2 = 0.82$ (from the regression analysis)

2.1.3 Bond behaviour

The bond mechanism is the interaction between the reinforcement and the surrounding concrete which allows longitudinal forces to be transferred from the reinforcement to the surrounding concrete.

Bond for plain bars includes three components: chemical adhesion, micromechanical interaction associated with rough steel surface and friction after slip. The bond for deformed bars depends primarily on mechanical action, the chemical and physical adhesion play a minor role[33].

The bond interaction between the concrete and a bar subjected to a pull-out force is characterized by four different stages [34]:

Stage Ⅰ (uncracked concrete): For low bond stress values, $\tau \leq \tau_1$=（0.2-0.8） $f_{c,sp}$, where $f_{c,sp}$ is the tensile strength; bond efficiency is assured mostly by chemical adhesion.

Stage Ⅱ (first cracking): For higher bond stress values ($\tau > \tau_1$), the chemical adhesion breaks down; in deformed bars the lugs induce large bearing stresses

Stage Ⅲ for still higher values, τ > (1-3) $f_{c,sp}$

Stage Ⅳa for plain bars, this stage follows the breakage of the adhesive bond, force transfer is provided by friction

Ⅳb Bond stress values as high as (1/3-1/2) f_c can be developed, where f_c is the compressive strength. The longitudinal cracks (splitting cracks) occur through the whole cover.

Ⅳc Bond failure is caused by bar pull-out in the case of deformed bars confined by heavy transverse reinforcement.

Depending on the type of interaction between the bars and concrete, there are two types of bond failure: pull-out failure and splitting failure. In the former case, bond failure is due mostly to the shearing-off of the concrete keys cast between each pair of lugs. In the latter case, bond failure is due mostly to the longitudinal splitting of the concrete surrounding the

bar. However, in practice a more complex failure mode is exhibited, which can be summarized as follows [34]:

Pull-out failure with no or partial concrete splitting (no visible splitting cracks): high confinement and /or large concrete cover; shearing off of the concrete keys;

Pull-out failure induced by partial splitting or through splitting (visible splitting cracks): moderate confinement and/or limited concrete cover; shear-off of the concrete keys accompanied by concrete slip on rib faces. Normally this is called splitting-induced pull-out failure.

Splitting failure induced by spalling of the cover: no confinement and/or very limited cover with bar slip on rib faces

The resultant compressive force exerted by the ribs on the concrete is inclined at an angle to the bar axis. The radial component of this force creates a ring of tension in the concrete that envelops the bar (Figure 2.2)[33]. If the tension force generated by the bond action exceeds the capacity of the ring, bond failure occurs due to the splitting of the concrete cover. If the cover is greater or if the sufficient confining reinforcement or transverse pressure opposes the splitting force, a pull-out type of failure develops with the concrete being sheared on a surface across the top of the ribs.

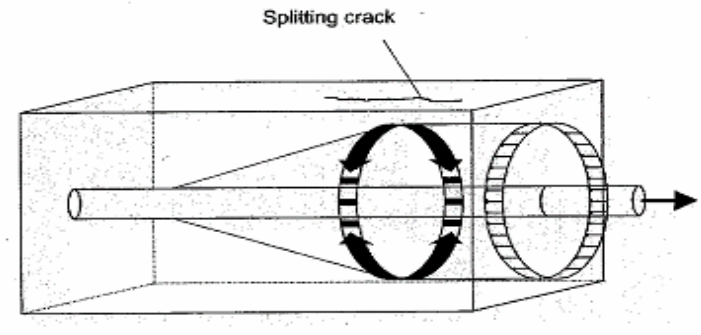

Figure 2.2 Tafel ring

As presented later in this thesis, splitting failure and splitting-induced pull-out failure were observed on specimens with C/Φ=1 and C/Φ=3.

Previous research has shown that bond behaviour depends on a variety of factors and parameters. These include: the properties of the reinforcement, concrete strength and the stress state in both the bars and the surrounding concrete, the concrete cover, casting direction with respect to bar orientation, and bar size.

Figure 2.3 illustrates the potential consequences of reinforcement corrosion on residual strength [34]. As mentioned in Chapter 1, the residual strength of a concrete structure may be affected by local or general loss of the reinforcement cross section, through cracking or spalling of concrete or through the loss of bond. The corrosion of reinforcing bars can greatly influence the bond strength. Cracking occurs due to the expansion of corrosion products on the bar surface. Any spalling resulting in loss of concrete cover results in a loss of confinement and a reduction in bond strength at the interfacial zone between the two materials. The soft layer on the bar surface formed by the accumulated corrosion products effectively reduces the friction component of the bond strength. Moreover, the deterioration of the ribs of the deformed bars causes a significant reduction of the mechanical interaction force, which is a major component of the bond strength of deformed bars. Hence the bond strength decreases significantly.

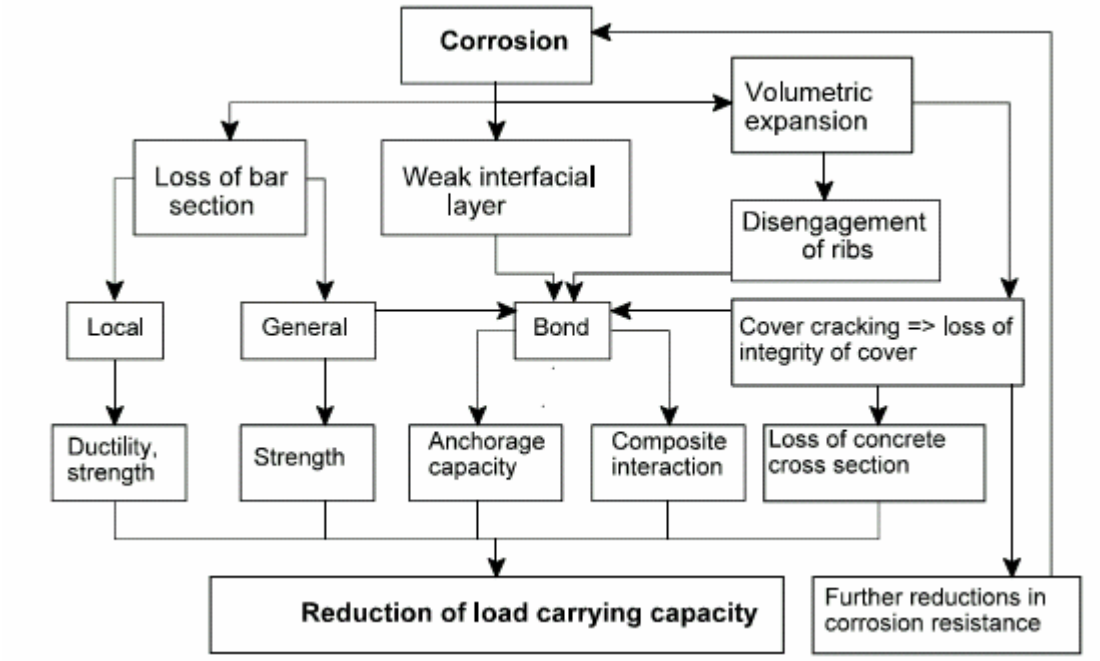

Figure 2.3 Effects of corrosion on residual strength

Bond behaviour in corroded reinforced concrete can be assessed in the laboratory by including salt (NaCl) in the mix to activate the corrosion process and by accelerating the process by applying an impressed current. Whilst several factors have been found to affect bond strength loss, it is hard to compare such results as a variety of experimental methods have been used. Published test data shows differences due to a variation in test specimens and different current densities. This issue is discussed further in the Methodology chapter (Chapter 3).

Much of the existing research [13, 15-17, 20, 23, 35, 36] has reported similar patterns of change of bond strength as corrosion develops, as typified by Figure 2.4. The bond strength is seen to increase by a small amount, when corrosion is at its initial stage, but reduces as corrosion increases. The increase of internal pressure caused by the development of expansive corrosion products before cracking occurs increases the confinement and mechanical interlocking of the concrete around the bar. Secondly, the roughness of the bar is also increased, thereby enhancing the friction between the bar and the surrounding concrete.

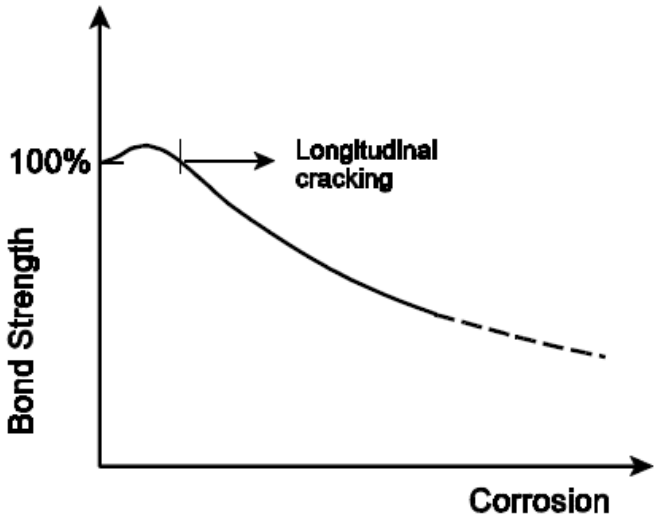

Figure 2.4 Variation in bond strength with corrosion (Schematic)

2.2 Preliminary investigations

To determine the criteria for different extent of corrosion as a function of crack width, two prototype specimens were cast. Crack widths of 2 mm were observed to result in spalling or very near spalling conditions in unconfined concrete (without stirrups) with a cover of one bar diameter ($C/\Phi = 1$). This result has been reported by other researchers [1, 11]. A mix design with a water/cement ratio of 0.5 and a target strength of 40 MPa has been adopted for the work reported here.

The concrete design comprised normal Portland cement, fine aggregate (medium-sized natural sand) and crushed coarse aggregate. The ratio by weight of cement/sand/coarse aggregate was 182:247:442, with a water/cement ratio of 0.49 (refer to Table 3.2).

Initially, three corrosion stages were adopted. These were average surface crack widths of 0.05, 1 and 1.5 mm. However, because it was hard to control the exact crack width, the target

crack widths were used only as a guide. Subsequently, extra specimens were tested for a target crack width of 0.5 mm. In addition control specimens were cast that did not undergo accelerated corrosion. These control specimens still underwent corrosion as they were cast with salt in the mix. These specimens were examined following pull-out testing to determine section loss in the same way as for the accelerated bars. Thus results were obtained for a stage of corrosion referred to as non-cracked.

3 Methodology

3.1 Design of specimens

3.1.1 General

All the specimens were cast in the RMIT concrete laboratory at room temperature. Detailed material information is listed in Table 3.1. The tensile strength of the Φ12 mm and Φ16 mm steel bars used is nominally 500 MPa, which equates to a failure load of 56.5 kN and 100.5 kN respectively.

Materials	Specification
Coarse Aggregate	Pioneer Quarry in Kilmore
Sand	Alex Quarry (initially) then Bulla Quarry
Steel	SMORGAN Normal ductility with 500 MPa yield strength
Salt	CHEETHAM Salt limited Crown P.D.V Salt No.1

Table 3.1 Material information

The sand source was changed because of supply difficulties. An initial replacement sand resulted in a higher compressive strength (batch f and k) (refer to Table 4.4). Following this a sand with similar grading to the original was adopted and control mixes were used to produce concrete of similar strength (batch h) (refer to Table 4.4).

Table 3.2 gives the concrete mix details. As mentioned in Chapter 2.1.1, 3% salt (NaCl) by weight of cement was added to assist with the corrosion process.

Material	Cement	w/c	sand	10mm washed aggregate	7 mm washed aggregate	Salt	Slump
Quantity	381 kg/m3	0.49	517 kg/m3	463 kg/m3	463 kg/m3	18.84 kg/m3	140 25 mm

Table 3.2 Concrete mix design

Cylinders were cast to assess concrete strength. 100 mm diameter cylinders for compressive

strength and 150 mm diameter cylinders for indirect tensile strength [37] (Figure 3.1 and Figure 3.2).

Figure 3.1 Compressive test

Figure 3.2 Tensile strength test

Steel bars of Φ12 mm and Φ16 mm with normal ductility and 500 MPa yield strength were used in this study. All bars were of identical rib geometry as shown in Figure 3.3 [38].

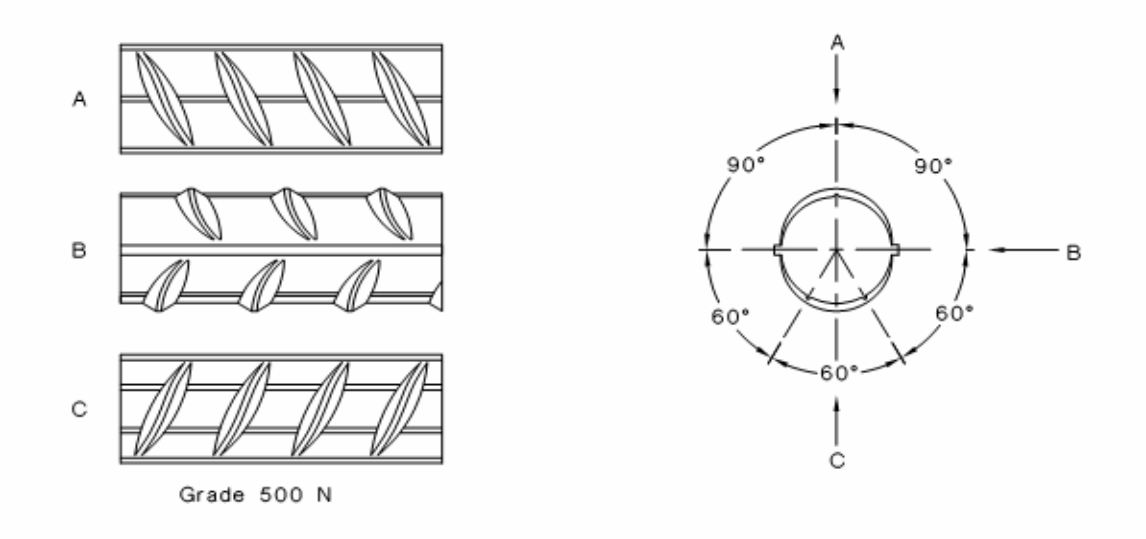

Figure 3.3 Rib geometry of Grade 500 N steel reinforcing bars

The bars were initially cleaned to remove any weathered corrosion products, so as to enable the mass loss of corrosion products induced by accelerated corrosion to be assessed by comparing the initial and final weight. The bars were cleaned with a 12% hydrochloric acid solution, then washed in distilled water and neutralized by a calcium hydroxide solution before being washed in distilled water again. Following the pull-out test, the corroded bars were cleaned in the same way and weighed again [20]. The average corrosion penetration was

calculated using Equation 2.2. The weight loss due to corrosion was assessed by calculation based on time and current of corrosion comparing with actual mass loss.

3.1.2 Selection of test models

The choice of the type of specimen for bond strength evaluation is critical because it influences the bond performance. Different types of tests include: cubic concentric pullout tests, tension pullout test, bond beam test and cantilever bond test. These may be simply divided into two categories namely “pullout tests” and “flexural tests” [36].

The RILEM concentric pullout test [39] (Figure 3.4) is well recognised because of its simplicity and is often used to determine the bond slip characteristics for use in finite element modelling [11]. Disadvantages are that the concrete surrounding the steel bars is in compression when the bar is pulled in tension, creating an unrealistic situation when compared to flexure; In addition, splitting failure is difficult to observe in this test. The tension pull-out test on beams or slabs was developed to simulate concrete in tension. Although there has been effort made to achieve a standard test [40], there is no test specimen or loading style that fully represents the actual bond behaviour in real structures. However, having considered the cost and simplicity, the beam end specimen [11, 25, 41, 42] was selected for this study. The test eliminates compression on the concrete specimens and results in bond strength values representative of the splitting failure modes considered by design Codes of Practice [41].

This type of eccentric pullout or ‘beam end’ type specimen uses a longer bonded length representative of the anchorage zone of a typical simply supported beam. Specimens of rectangular cross section were cast with a longitudinal reinforcing bar in each corner and without stirrups (Figure 3.5).

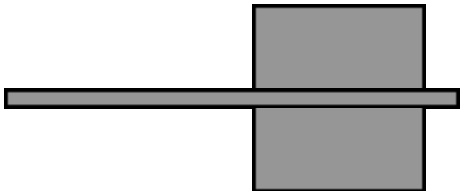

Figure 3.4 RILEM concentric pullout specimen

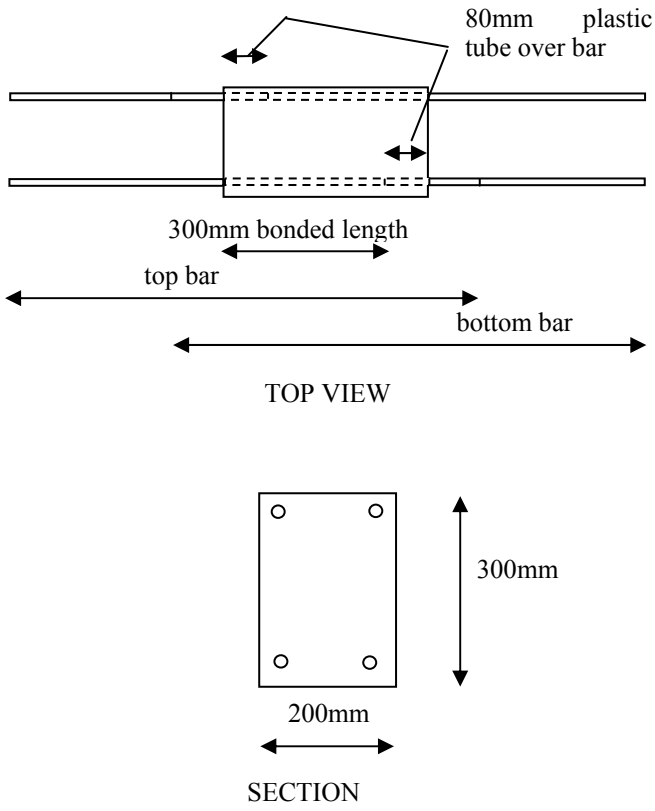

Figure 3.5 Sketch of adopted beam end specimen

Four groups of specimens (Table 3.3) were cast with different bar diameter and cover/diameter (C/Φ) ratios in order to investigate size effects and the influence of C/Φ on the loss of bond strength.

Bar diameter(mm)	C/Φ Ratio	Specimen No.
12	1	5
	3	4
16	1	7
	3	9

Table 3.3 Specimen specifications

3.2 Testing procedure

After the period of accelerated corrosion, the bars were pulled out of the specimens and the peak pullout (bond) strength was measured. The loaded end slip and free end slip was assessed using an LVDT. All data was record by a DATATAKER.

3.2.1 Calibration of equipments

The electrical/electronic equipment (LVDTs and load cell) used in the pullout test were calibrated as follows.

An LVDT (RS components: SDCR15 with a sensitivity of 265mv/mm at 10V and response time 0.4ms) was used at the loaded end of the bar and calibrated at 15V DC (Figure 3.6).

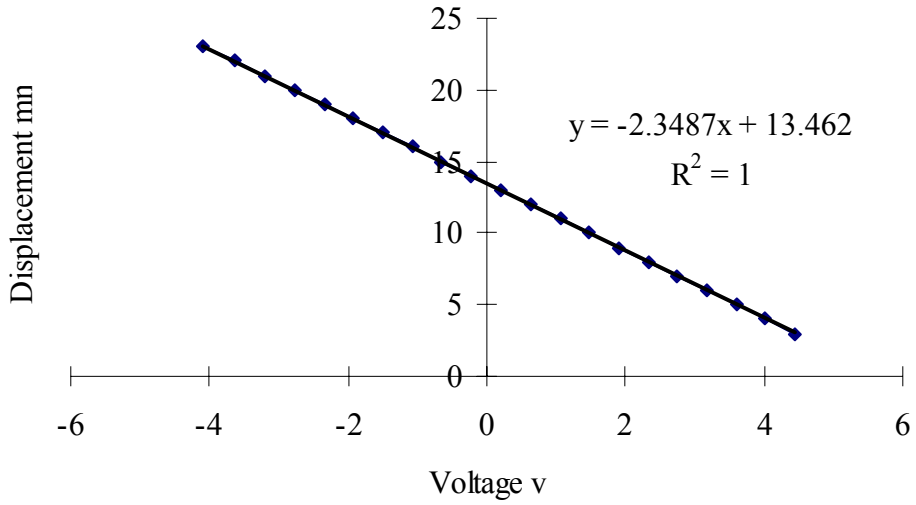

Figure 3.6 Calibration curve at loaded end LVDT

An LVDT (SOLARTRON DG/5.0 with a sensitivity of 540mv/mm at 10V and response time 5ms) was used at the free end and calibrated at 15V DC (Figure 3.7).

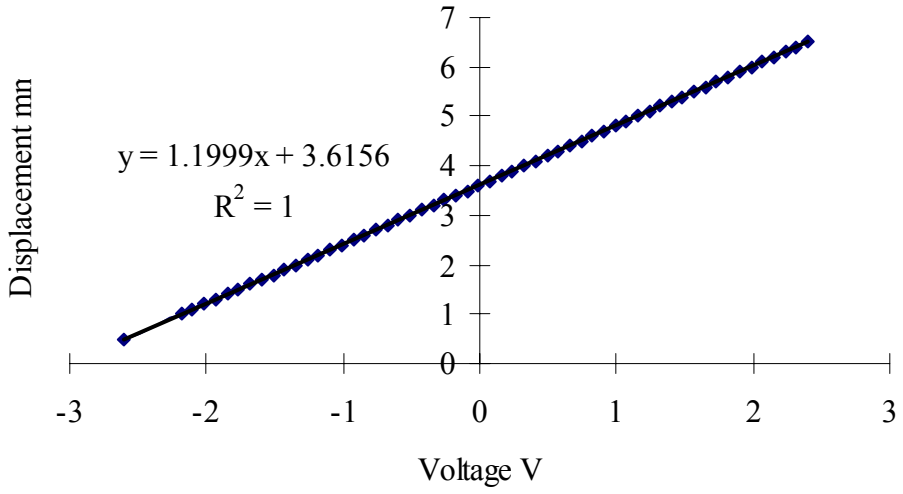

Figure 3.7 Calibration curve of free end LVDT

Figure 3.8 shows the calibration curve of the load cell and calibrated on 10 V DC.

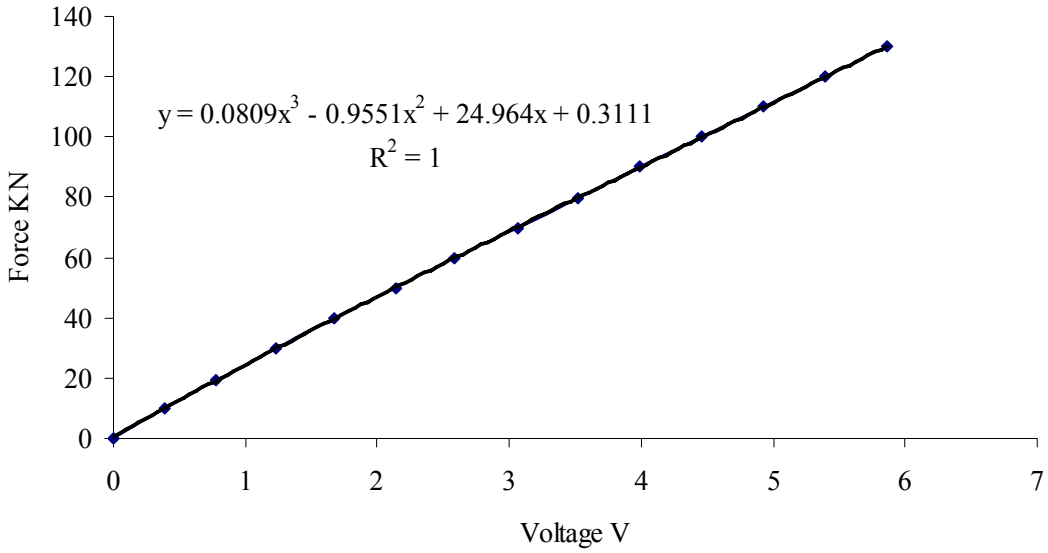

Figure 3.8 Calibration curve of load cell

3.2.2 Accelerating corrosion

To accelerate the corrosion process, a current was applied using a power supply to maintain a constant current under varying voltage. The steel bars served as the anode and four metal plates were fixed on the surface to serve as cathodes. Sponges (sprayed with salt water) were placed between the metal plates and concrete to provide an adequate contact (Figure 3.9).

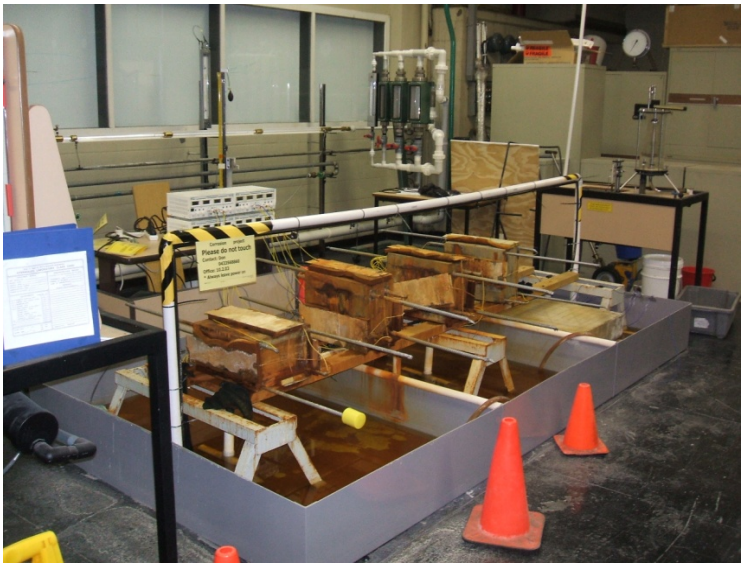

Figure 3.9 Accelerating system

A current density of 200 μA/cm^2 was applied to the bars in pairs (top pair and bottom pair), with each pair being wired in series with a power supply maintaining the constant current flow. When the required crack width was achieved for a particular bar, that bar was removed from

the circuit and the current adjusted accordingly to maintain the required current density. A 3% salt water spray was applied under a “one day wet” and “two days dry” cyclic regime to simulate the tide environment. The corrosion process was halted (the current disconnected) when the crack width achieved the predetermined magnitude. The specimen was removed for pullout testing when all four locations exhibited the target crack width. The surface crack width was regularly measured at 20 mm intervals, beginning 20 mm from the end of the plastic tube (bond breaker) by using microscopy with an accuracy of 0.02 mm. Measurements were taken normal to the bar direction. A method using digital image analysis was considered to provide more accurate measurement. However, due to the corrosion staining, it was difficult to identify the boundary of the cracks clearly. This would be worthy of future investigation.

3.2.3 Pull-out system

Bond strength tests were conducted by means of a hand operated hydraulic jack and a custom-built test rig as shown in Figure 3.10. The loading scheme is illustrated in Figure 3.11 [11]. A plastic tube of length 80 mm was provided at the end of the concrete section underneath the transverse reaction to ensure that the bond strength was not enhanced by this reactive force.

The specimen was set up so that an axial force was applied to the bar being tested. The restraints were sufficiently rigid (based on pre-test calculations) to ensure minimal rotation or twisting of the specimen during loading.

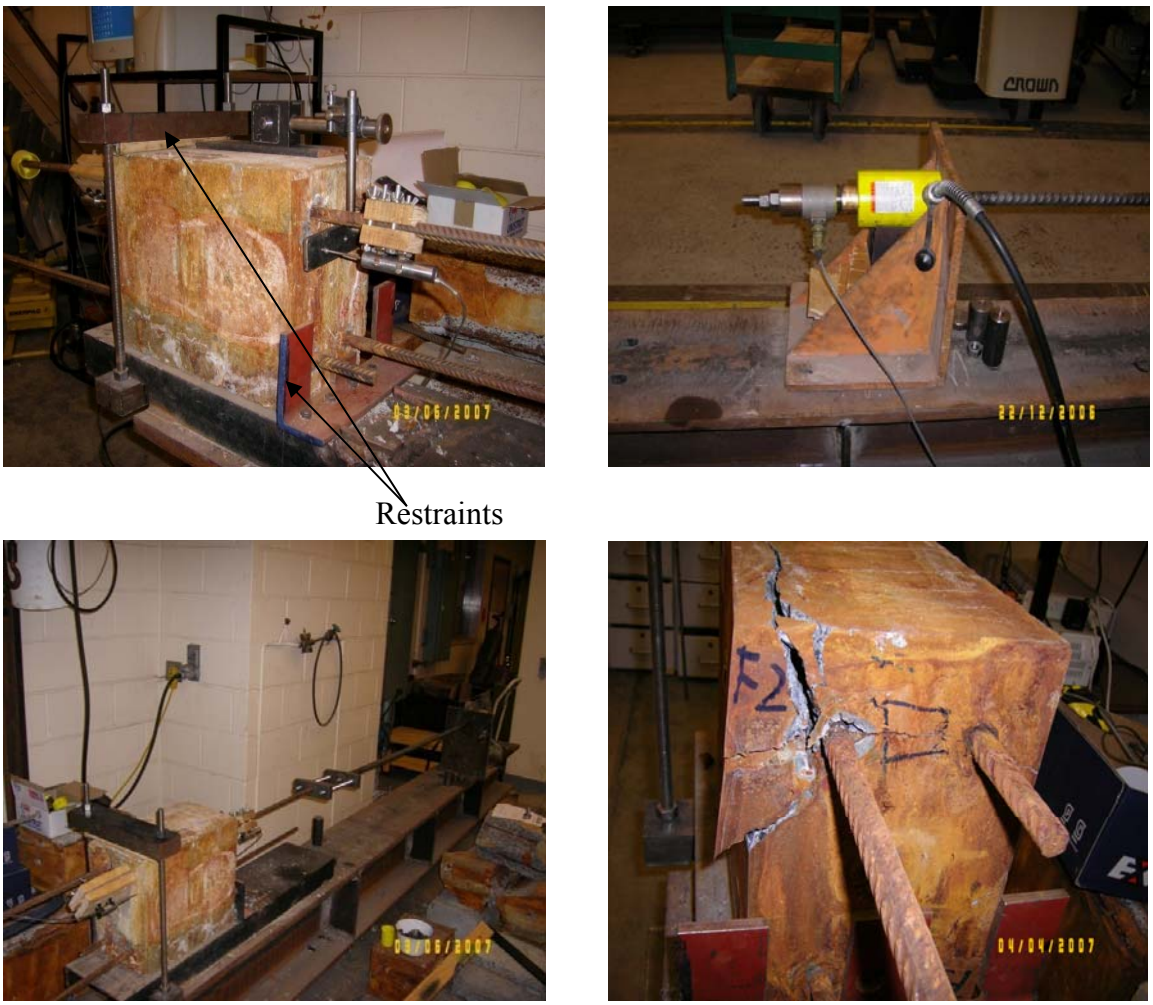

Figure 3.10 Pull-out test

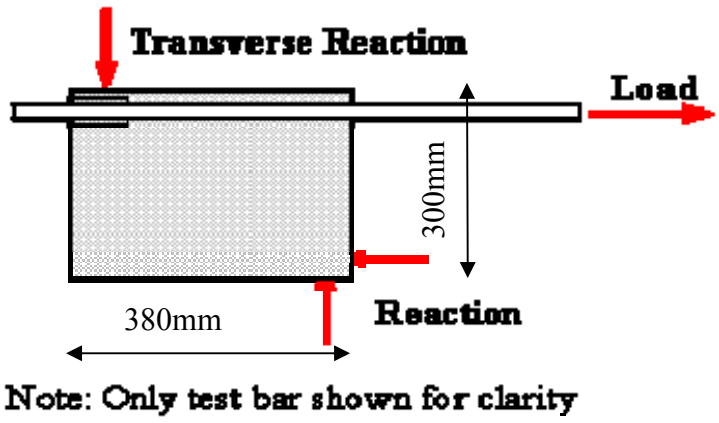

Figure 3.11 Loading scheme

4 Test results

4.1 Analysis of concrete compressive strength

A concrete mix designed for a characteristic strength of 40 MPa was used. However, due to the many factors affecting the quality of concrete, it is difficult to achieve the same compressive strength from batch to batch. A significant issue was the change of supplier of the sand – even though the grading was similar. The mean compressive strength achieved for the initial mix was 38 MPa with a standard deviation 2.63 (Table 4.1) and the average tensile strength was 3.05 MPa with a standard deviation of 0.36 (Table 4.2). The concrete strength was tested at the time of the pullout tests. There were two batches for specimens using the later mix for groups 3 and 4 with a compressive strength of 50 MPa (Table 4.3)

Group No.	Specification	Numbers of Specimens	Compressive strength (MPa)	Average compressive strength MPa	Standard deviation
1	12 mm, 1 C/Φ	5	36.0~ 37.0	38	2.63
2	12 mm, 3 C/Φ	4	34.0~38.0		
3	16 mm, 1 C/Φ	5	36.5~42.5		
4	16 mm, 3 C/Φ	7	38.0~42.5		

Table 4.1 Compressive strength for 40 MPa specimens

Group No.	Specification	Numbers of Specimens	Tensile strength (MPa)	Average tensile strength MPa	Standard deviation
1	12 mm, 1 C/Φ	5	2.89, 2.69	3.05	0.36
2	12 mm, 3 C/Φ	4	2.71, 2.96		
3	16 mm, 1 C/Φ	5	2.83		
4	16 mm, 3 C/Φ	7	2.99, 3.02		

Table 4.2 Tensile strength for 40 MPa specimens

Group No.	Specification	Numbers of Specimens	Compressive strength (MPa)	Tensile strength (MPa)
3	16 mm, 1 C/Φ	2	50	4.04
4	16 mm, 3 C/Φ	2	50.5	3.55

Table 4.3 50 MPa specimens

Table 4.4 gives the detailed information for each batch. The original mixer only allowed two specimens to be cast per batch. However the mixer was replaced later by a larger mixer which was used for Batch h (the final cast).

Figure 4.1 shows the relationship between concrete compressive strength and relative tensile strength. A clear trend can be observed with the tensile strength being approximately 8 % of the compressive strength.

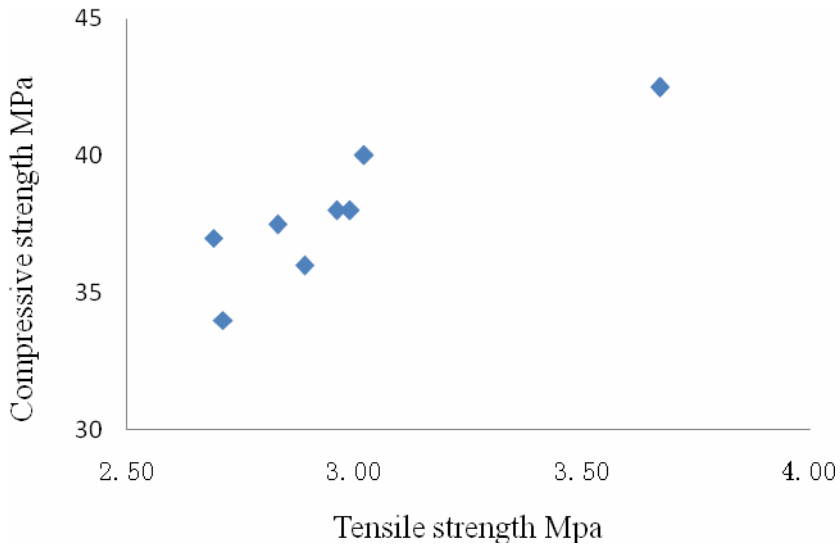

Figure 4.1 Compressive strength vs tensile strength

Concrete is a brittle material, and week in tension, any internal crack or void may significantly influence the results. For this reason, it is more reliable to use the compressive strength, rather than tensile strength as quality control.

Group NO.	Designed crack width stages mm	Specified batch	Compressive strength MPa	Tensile strength MPa
1	0	a	36.5	N/A
	0	b	37	2.69
	0.5			
	1	c	36	2.89
	1.5			
2	0	d	38	2.96
	0.05			
	1	e	34	2.71
	1.5			
3	0	f	50	4.04
	0.05			
	0	g	37.5	2.83
	0.05			
	0.5	h	42.5	3.67
	1	i	36.5	N/A
	1.5			
4	0	j	40	3.02
	0.05			
	0	k	50.5	3.55
	0.05			
	0	h	42.5	3.67
	0.05			
	0.5			
	1	l	38	2.99
	1.5			

Table 4.4 Detailed information of cast concrete

Compressive strengths and tensile strengths play a major role in pull-out and splitting failures respectively. The less than linear dependence of bond action on concrete compressive strength

had been reported by Martin and Noakowski [43]. Many other researchers [14, 27, 41, 44-46], have suggested that bond stress tends to increase proportionally with the square root of the concrete compressive strength, and Stanish and Anyeung use this to interpret bond strength for corroded specimens. However, there is no published evidence that bond strength is related to the square root of the compressive strength for corroded specimens. Therefore, the bond strength are analysed here for specimens that have similar compressive strength (Table 4.1).

4.2 Extent of corrosion

4.2.1 Assessment of extent of corrosion

The expressions for bar diameter loss (attack penetration) and mass loss have been compared to bond strength loss.

For diameter loss, Equation 4.1 derived from Equation 2.1 and 2.2 has been used to calculate bar diameter percentage loss (corrosion level) by other authors [14, 26]**.**

$$C_r=2RT/\Phi\% \qquad 4.1$$

Where C_r is bar diameter loss in percentage, R is material loss equals 1.156 cm/year, T is time of corrosion and Φ is bar diameter.

Equation (4.2) derived from Andrade's work [2] has been used to express loss of diameter as corrosion develops further.

$$\Phi\ (t) = \Phi\ (i) - 0.023IT \qquad 4.2$$

Where Φ (t) is the bar diameter(mm) at time t, Φ(i) is the initial bar diameter(mm), I is the current applied in $\mu A/cm^2$, T is the time of current flow, and 0.023 is the conversation factor ($\mu A/cm^2$ to mm/year) in the case of homogeneous corrosion. However, the current efficiency is not 100%, and current flows via other routes and not through the bars. Consequently measured mass loss (gravimetric mass loss) is a more reliable measure. Hence, the gravimetric mass loss was used in this project to represent the extent of corrosion (corrosion level).

The actual corrosion level was determined using the following equation (4.3):

$$C_R = \frac{(G_0 - G)}{g_0 l} \times 100\% \qquad 4.3$$

Where G_0 is the initial weight of the steel bar before corrosion, G is the final weight of the steel bar after removal of the corrosion products, g_0 is the weight per unit length of the steel bar (0.888 and 1.58 g/mm for Φ12 mm and Φ16 mm bars respectively), l is the embedded bond length.

4.2.2 Comparison of theoretical and actual mass loss

There are several reasons that might affect the actual mass loss results:

1. The efficiency of the current is not 100% due to stray current in the circuit.
2. The power supply used in this project did not have a sufficiently accurate means of setting the constant current. In addition the "constant current" fluctuated within a range of the preset value.
3. The disconnected bars which had already reached the target corrosion level (controlled by surface crack width) will continue to corrode even though no current is being applied. This corrosion rate could be as great as 100 μA/cm^2 (highest natural corrosion rate measured in the laboratory) by others [8, 22].
4. There are small regions of the steel bar (inclusions) that do not dissolve electrolytically but that spall out from the metal surface when the surrounding material is oxidizing[1]. This results in mass loss greater than calculated from current flow.

To minimize error, the actual mass loss data was assessed by adding the previous mass loss obtained from the controlled specimens (specimens that had not been through the wet-dry cycle and accelerated corrosion). These would have suffered mass loss due to natural corrosion due to the presence of chloride ions when the specimens were cast. The top bars and bottom bars were analysed together, because they were in pairs in the accelerating system.

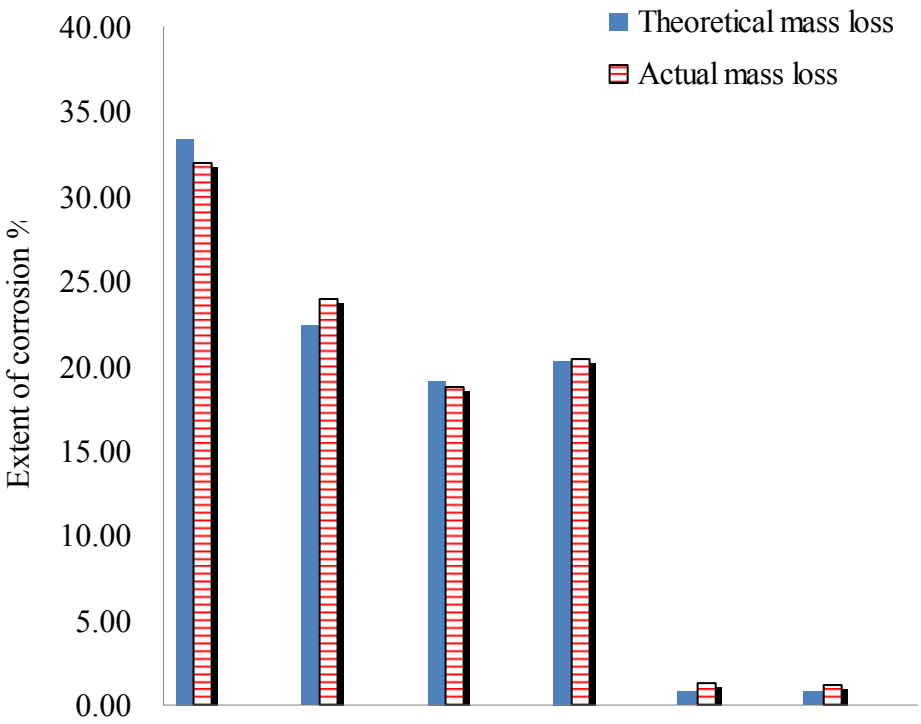

Figure 4.2 Comparison of theoretical mass loss and actual mass loss for the pairs of 12 mm bars with 1 C/Φ

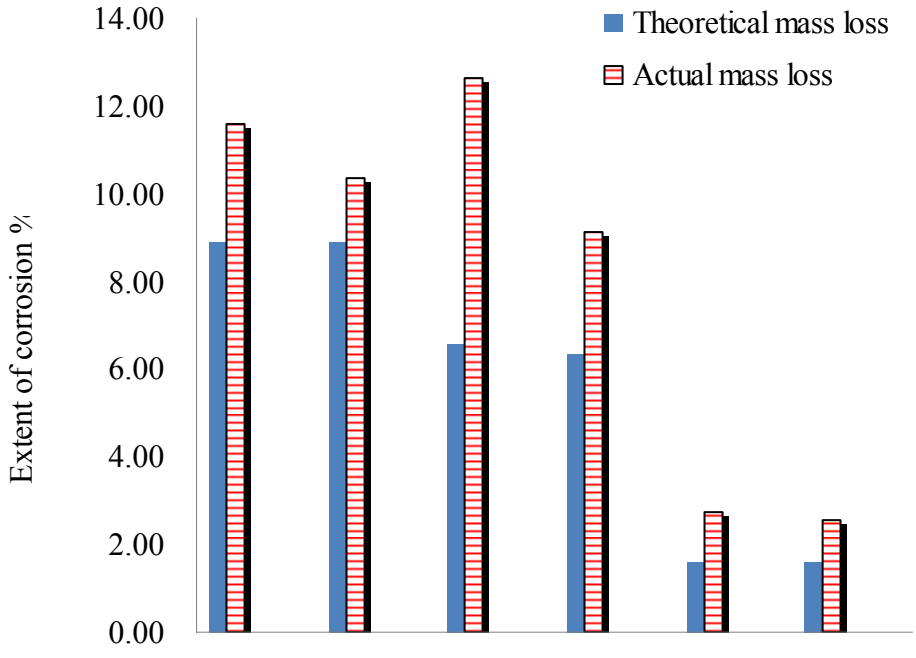

Figure 4.3 Comparison of theoretical mass loss and actual mass loss for the pairs of 12 mm bars with 3 C/Φ

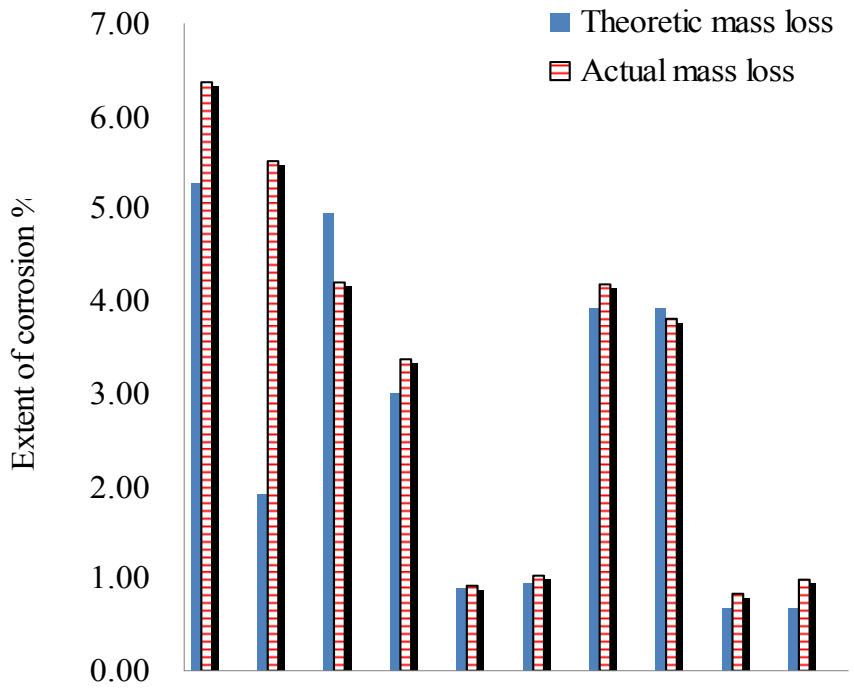

Figure 4.4 Comparison of theoretical mass loss and actual mass loss for the pairs of 16 mm bars with 1 C/Φ

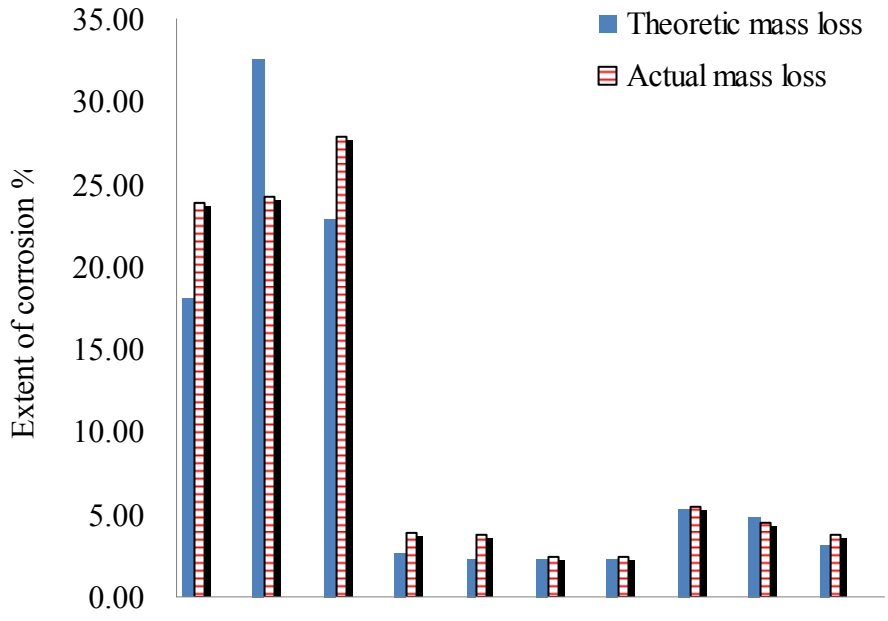

Figure 4.5 Comparison of theoretical mass loss and actual mass loss for the pairs of 16 mm bars with 3 C/Φ

Figures 4.2 - 4.5 show comparison of theoretical mass loss and actual mass loss. These results show that the actual mass loss in several cases was higher than the theoretical value. Similar findings have been reported by Alonso [1]. The difference between the theoretical mass loss (based on Faraday's law) and actual mass loss (based on gravimetric mass loss) can be

attributed to the errors described above.

4.3 Bond strength of corroded reinforcement

4.3.1 Assessment of bond strength

Depending on the assumption that bond stress is uniform along the embedded length [47, 48], bond strength at any stage of loading is determined by simply dividing the load by the embedded area of the bar. Hence, the average peak bond strength can be calculated by dividing the ultimate pullout force by the embedded surface area of the bar.

4.3.2 Influence of testing sequence

In several specimens, the overall damage caused by a pull-out test was so significant that subsequent pull-out tests would have been unreliable and hence such tests were rejected. This happened most frequently on the bars with higher cover and for corroded specimens. This is attributed to the cracks forming between adjacent bars. Splitting failure (Figure 4.6) and splitting-induced pull-out failure (Figure 4.7) were observed.

Figure 4.6 Splitting failure

Figure 4.7 Splitting-induced pull-out Failure

4.3.3 Experimental results of bond strength with related cracks and corrosion extent

The method of measuring cracks is covered in Chapter 3.2.2. Both average surface crack width and maximum surface crack width were measured to allow comparison with the change of bond strength. Tables 4.5-4.8 show the relationship between the extent of corrosion and crack size on bond strength. Note that the results for zero crack width refer to the control specimens in which non-accelerated corrosion occurred due to the addition of salt to the mix.

There is a variation in extent of corrosion exhibited by the control (non-cracked) specimens (Table 4.5). This is due to a varied time between casting and testing (discussed later in Section 5.7).

Bar Position	Average Surface crack width (mm)	Maximum surface crack width (mm)	Bond Strength (N/mm2)	Extent of corrosion (%)
T	0.000	0.00	3.087	0.52
T	0.000	0.00	3.5	0.42
T	0.000	0.00	4.017	1.47
T	0.000	0.00	3.646	1.25
T	0.048	0.08	3.289	1.35
T	0.059	0.08	3.806	1.33
T	1.130	2.40	1.453	36.95
T	0.983	1.80	2.4	18.22
T	1.360	2.50	0.905	26.72
T	1.248	2.18	1.379	19.10
B	0.000	0.00	3.617	0.33
B	0.000	0.00	3.499	0.46
B	0.000	0.00	4.279	1.29
B	0.000	0.00	3.13	1.52
B	0.042	0.09	3.421	1.19
B	0.049	0.08	2.956	1.07
B	1.022	1.86	2.53	24.27
B	1.119	2.06	2.006	16.39
B	1.207	2.00	1.685	16.70
B	1.160	1.58	1.742	28.74

Table 4.5 12 mm reinforcement with 1 C/Φ

Bar Position	Average Surface crack width (mm)	Maximum surface crack width (mm)	Bond Strength (N/mm2)	Extent of corrosion (%)
T	0	0	8.428	0.41
T	N/A	N/A	6.941	2.95
T	0.19	0.42	6.813	2.53
T	0.739	1.48	3.454	11.96
T	1.164	1.92	2.877	11.17
T	1.758	2.62	0.499	6.88
B	0	0	8.286	0.39
B	0.36	0.46	5.15	2.73
B	0.22	0.32	6.337	2.4
B	0.37	0.62	4.856	10.31
B	0.648	1.44	3.859	10.42
B	1.426	2	1.876	8.93
B	1.436	2.02	2.475	9.31

Table 4.6 12 mm reinforcement with 3 C/Φ

Bar Position	Average Surface crack width (mm)	Maximum surface crack width (mm)	Bond Strength (N/mm^2)	Extent of corrosion (%)
T	0	0	2.951	0.44
T	0	0	1.78	0.37
T	0.078	0.12	3.339	1.01
T	0.068	0.1	3.155	0.83
T	0.583	0.8	2.459	4.38
T	0.932	1.2	1.437	4.04
T	1.703	2.50	1.462	7.07
T	1.434	2.30	2.182	5.68
B	0	0	3.224	0.39
B	0	0	3.101	0.32
B	0.048	0.06	2.56	0.94
B	0.044	0.06	3.332	1.13
B	0.668	0.96	2.722	3.51
B	0.65	1.1	2.578	4.1
B	0.868	1.22	1.494	3.15
B	0.897	1.6	1.561	3.58
B	1.45	2	2.32	5.4
B	1.77	2.96	2.173	5.62

Table 4.7 16 mm reinforcement with 1 C/Φ

Bar Position	Average Surface crack width (mm)	Maximum surface crack width (mm)	Bond Strength (N/mm^2)	Extent of corrosion (%)
T	0.463	0.88	3.162	30.02
T	0.877	1.84	3.563	18.49
T	0.000	0.00	8.062	N/A
T	0.000	0.00	7.591	0.58
T	0.058	0.18	6.883	2.24
T	0.096	0.16	4.565	2.69
B	1.316	2.54	2.574	10.8
B	1.643	2.40	2.479	21.94
B	0.379	1.10	4.889	3.46
B	0.000	0.00	7.531	N/A
B	0.000	0.00	7.835	0.47
B	0.230	0.64	5.699	2.65
B	0.205	0.48	4.619	4.66

Table 4.8 16 mm reinforcement with 3 C/Φ

4.4 Pit characteristics

Pit depth was measured by using a dial gauge with an accuracy of 0.001 mm (Figure 4. 8), a needle was fixed to the head of the apparatus to act as a probe and the area was assessed both as a circle and an ellipse. Pit volume was assessed as a cylinder, a dome and an ellipsoid. For heavily corroded bars, the diameter loss was measured rather than volume of pits.

Figure 4.8 Dial gauge for measuring pits depth

Figure 4.9 Non-corroded 16 mm bar

Figure 4.10 Corroded 16 mm bar with approximately 15% mass loss

Figure 4.11 Corroded 12 mm bar with approximately 5% mass loss

Figure 4.12 Corroded 12 mm bar with approximately 20% mass loss

Figure 4.13 Corroded 12 mm bar with approximately 30% mass loss

Figures 4.9-4.13 show steel bars with varying extent of corrosion over bonded length. Several exhibit visible pitting and others exhibit significant overall section loss. When comparing the effect of the corrosion penetration on loss of bond strength, the penetration for bars with a greater section loss was assessed in terms of diameter loss.

To compare the effect of section loss, the formula (4.2) was applied [3]

$$\Delta A_S = \frac{\pi}{4}(2\alpha x\Phi - \alpha^2 x^2) \qquad 4.2$$

Where Φ is the bar diameter (mm); α is the corrosion factor, α=2 for homogeneous corrosion and $4\langle\alpha\langle 8$ for localized corrosion - α=4 was taken in this project; x is pit penetration.

Figures 4.14-4.16 show the bond strength vs corrosion penetration and section loss for 12 mm bars with a cover of one diameter. Figures 4.17-4.19 show the bond strength vs corrosion penetration and section loss for 12 mm with 3 C/Φ. Figures 4.20-4.22 shows the bond strength vs corrosion penetration and section loss for 16 mm with 1 C/Φ. Figures 4.23-4.25 show the bond strength vs corrosion penetration and section loss for 16 mm with 3 C/Φ.

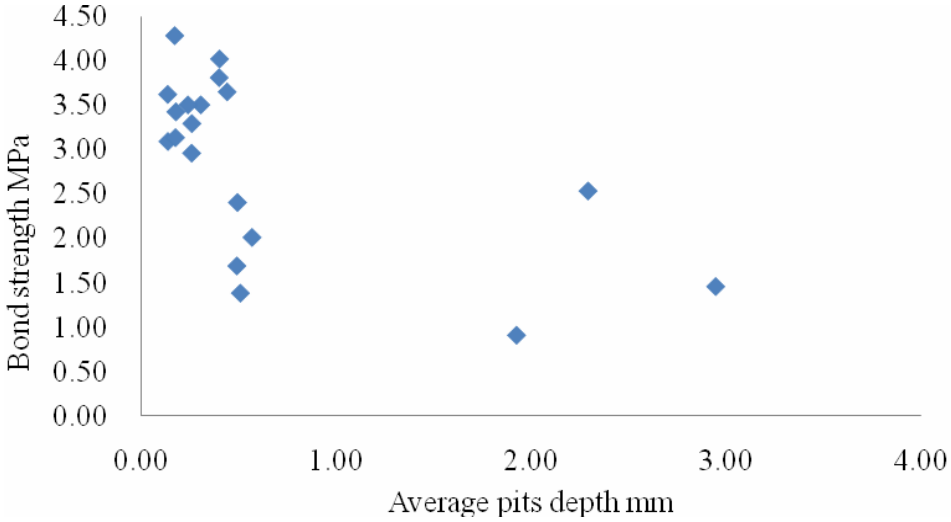

Figure 4.14 Bond strength vs average pits depth for 12 mm bars with 1 C/Φ

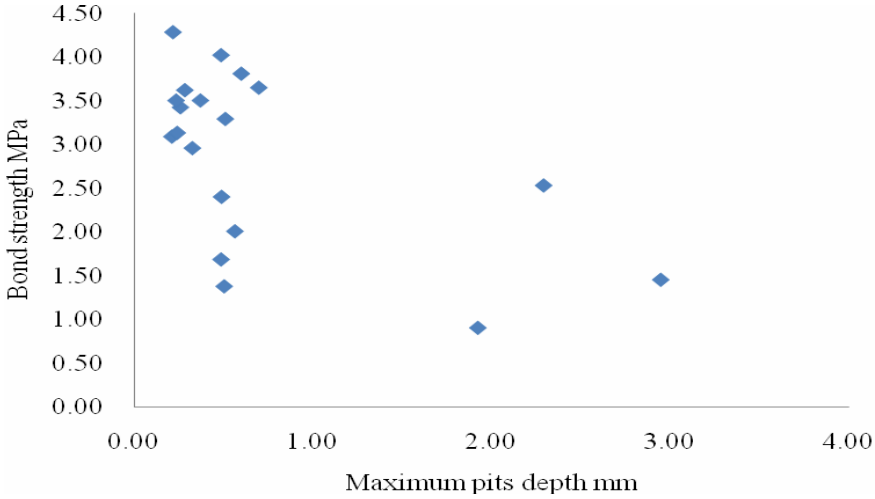

Figure 4.15 Bond strength vs maximum pits depth for 12 mm bars with 1 C/Φ

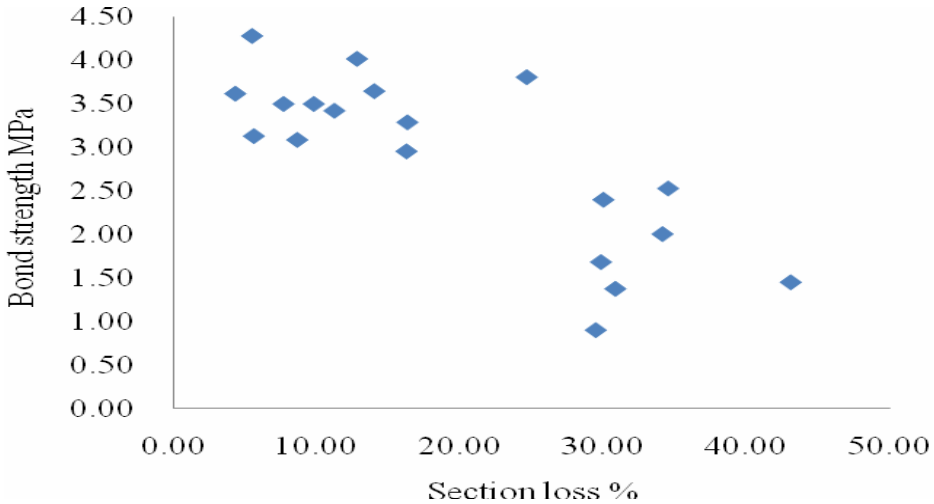

Figure 4.16 Bond strength vs section loss for 12 mm bars with 1 C/Φ

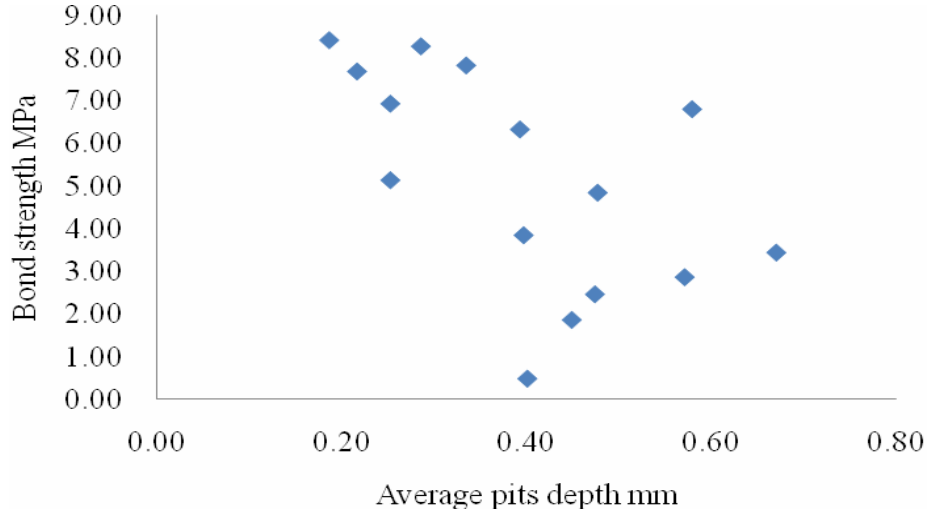

Figure 4.17 Bond strength vs average pits depth for 12 mm bars with 3 C/Φ

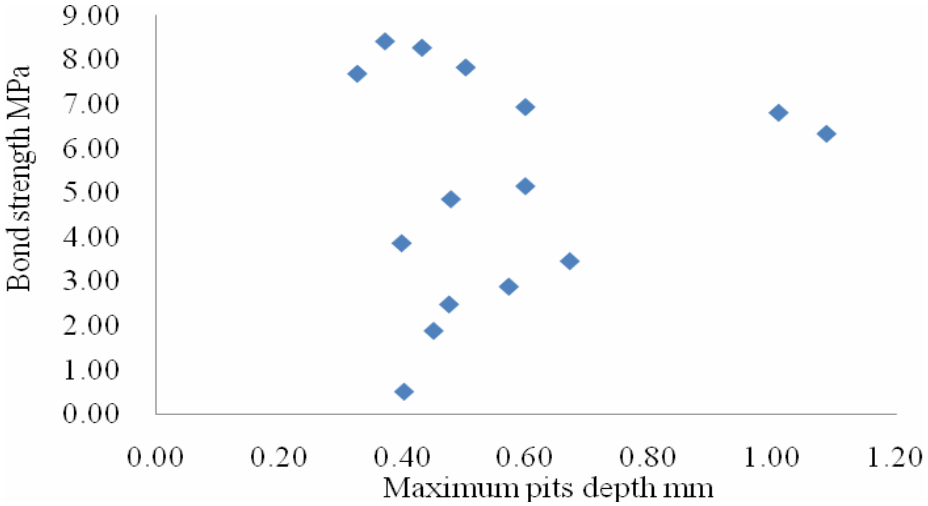

Figure 4.18 Bond strength vs maximum pits depth for 12 mm bars with 3 C/Φ

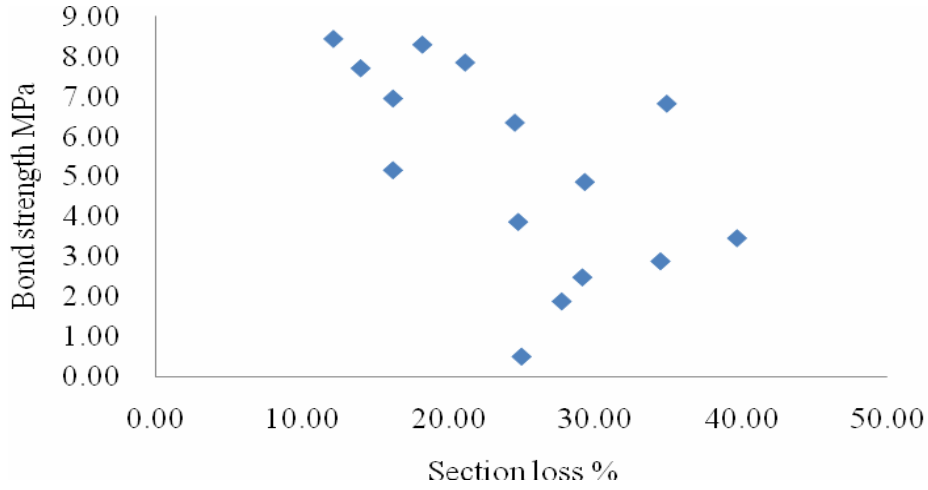

Figure 4.19 Bond strength vs section loss for 12 mm bars with 3 C/Φ

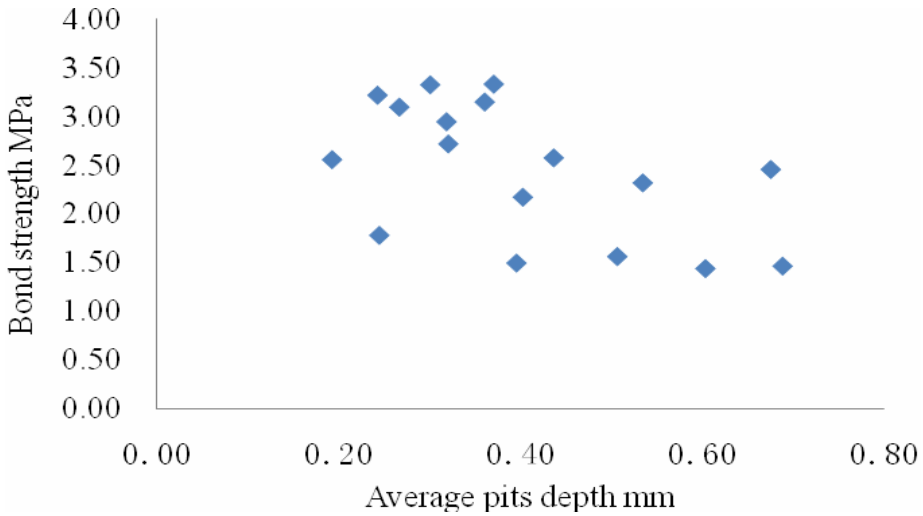

Figure 4.20 Bond strength vs average pits depth for 16 mm bars with 1 C/Φ

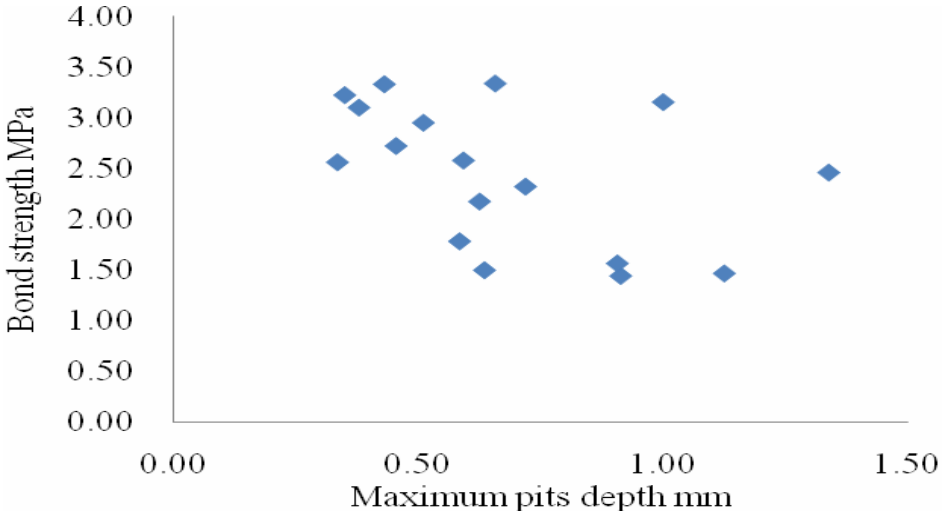

Figure 4.21 Bond strength vs maximum pits depth for 16 mm bars with 1 C/Φ

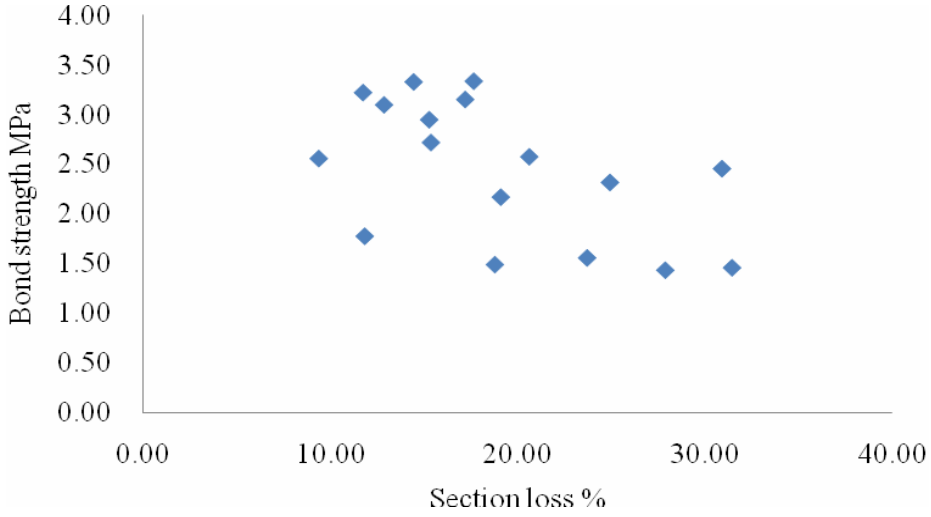

Figure 4.22 Bond strength vs section loss for 16 mm bars with 1 C/Φ

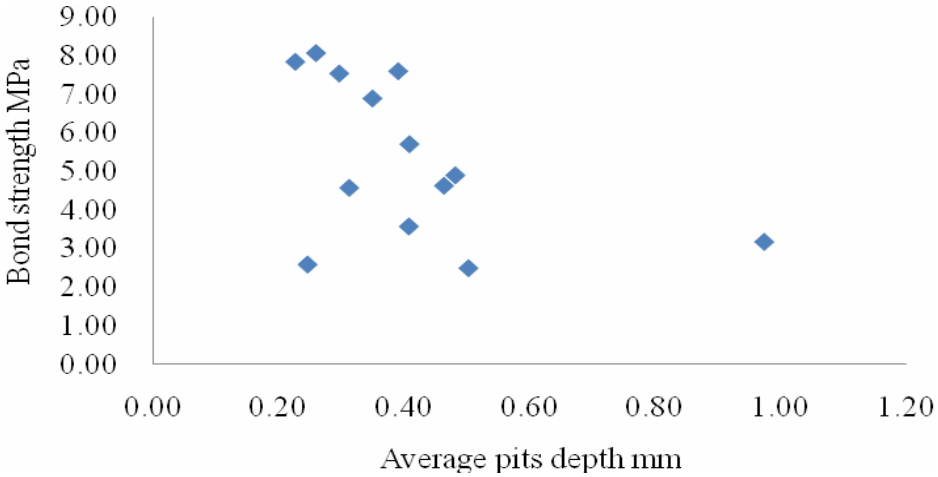

Figure 4.23 Bond strength vs average pits depth for 16 mm bars with 3 C/Φ

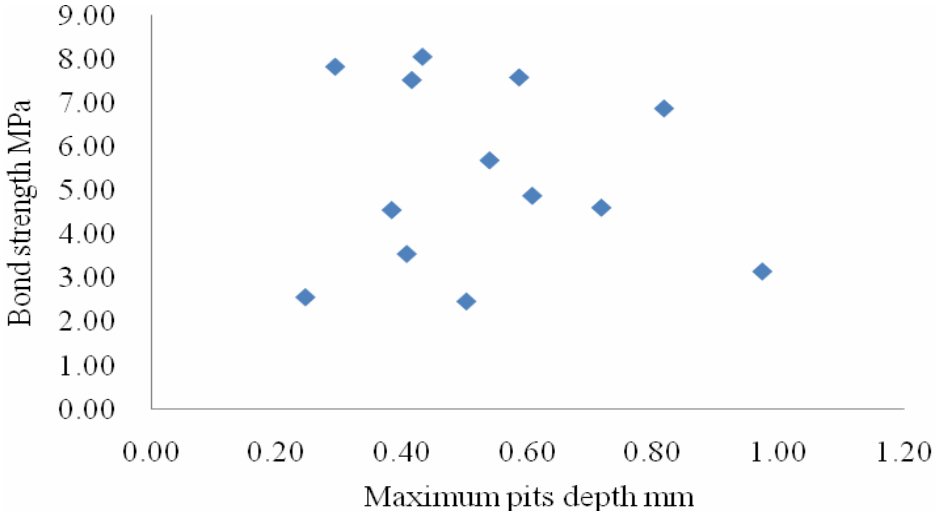

Figure 4.24 Bond strength vs maximum pits depth for 16 mm bars with 3 C/Φ

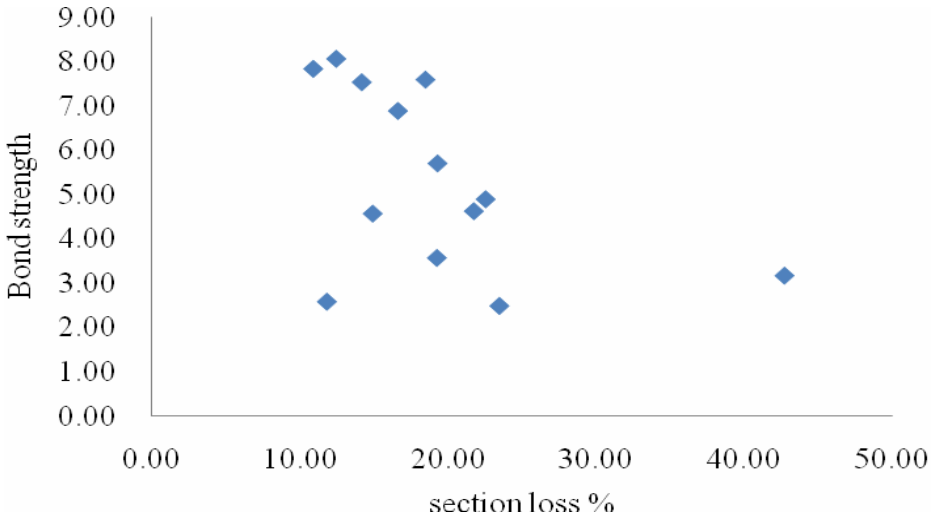

Figure 4.25 Bond strength vs section loss for 16 mm bars with 3 C/Φ

There is no clear trend demonstrated in Figures 4.14-4.25. However the results do give an indication that there is a reduction in bond strength with an increase of average pit depth and with section loss. Comparing the effect of pit depth on the bond strength, the figures show that the average pit depth provides a better relationship with bond strength rather than the maximum pit depth. The figures also show that the section loss tends to increase with increased bar size on bond strength loss.

Results show that the bond strength dropped more than 50% for Φ12 mm bars with a 20%-30% section loss. For Φ16 mm bars, the bond strength reduced 50% for a corresponding 10%-20% section loss.

The following sketch (Figure 4.26) shows the pits patterns observed on the surface of corroded bars. For low corrosion levels, the most common were single pits - with the covered pits, joined pits and honeycombed pits observed mainly on highly corroded bars.

Covered pits Joined pits single pit honeycombed pits single pit

Figure 4.26 Main pit pattern (top view)

4.5 Bond vs slip

The slip is defined as the relative difference in movement between the reinforcement bar and the concrete. The bond versus slip relationship dominates the performance of the structure and is affected by several parameters such as casting position, compaction of the concrete and loading rate.

The loading rate has a strong influence on bond stiffness and resistance [34]. Both loaded end slip and free end slip were continuously logged throughout the pullout tests. The loaded end results were found to be unreliable because of the slight lateral movement of bar at the loaded end which influenced the measurement of the attached LVDT. Therefore, only free end data have been interpreted here to analyse the effect of corrosion on bond slip. Due to the limitations of the testing equipment (in particular the manual hydraulic jack), it was difficult to apply a constant loading rate. Values of slip and load were recorded at 100 readings/s.

Typical curves for bond force versus slip are shown in Figures 5.16 and 5.17 (refer to 5.8.2 for details). Figures 4.27-4.30 show the relationship between pull-out force and free end slip for different extent of corrosion and the corresponding maximum slip at ultimate force.

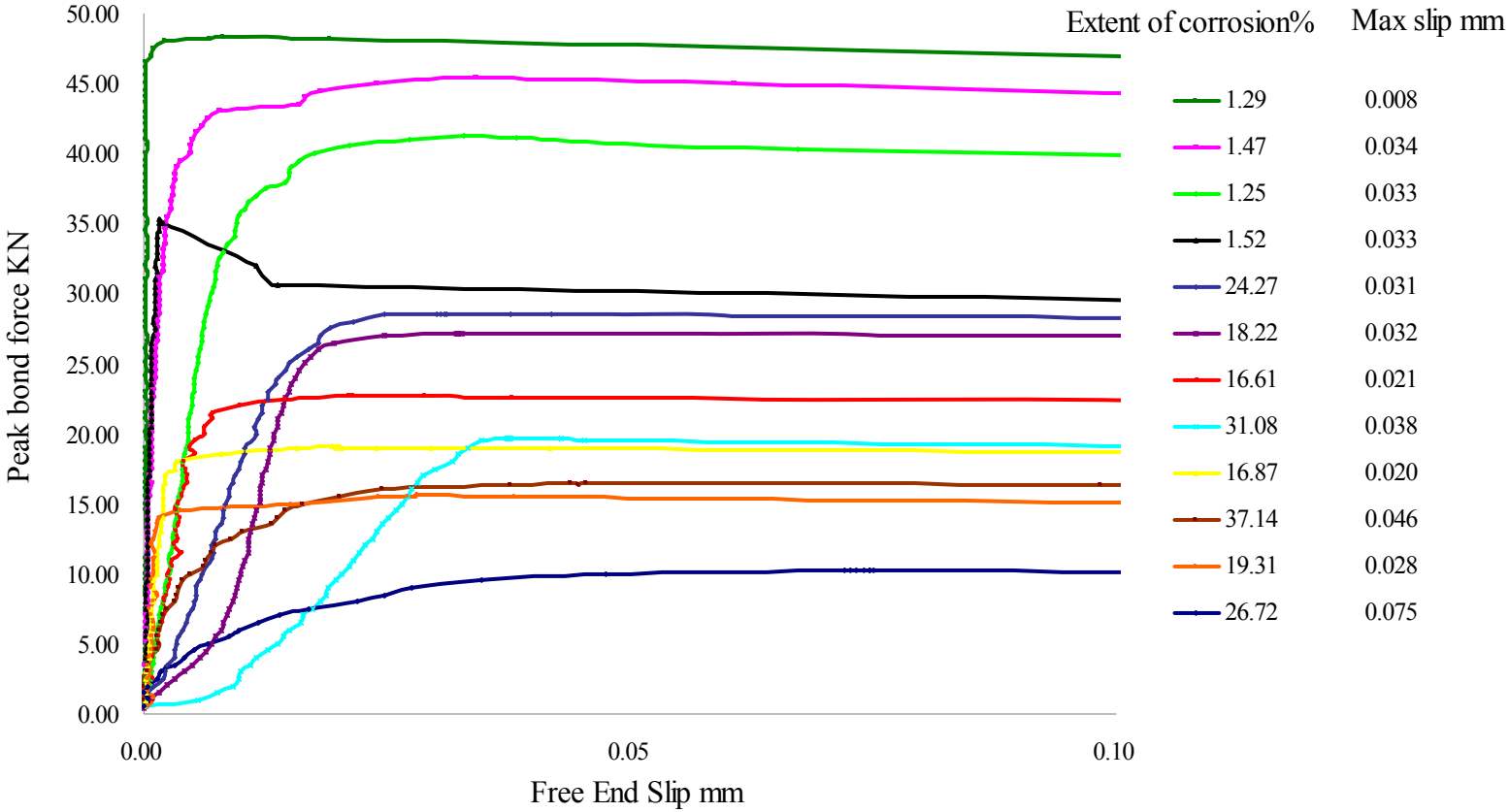

Figure 4.27 Peak bond force vs free end slip for 12 mm bars with 1 C/Φ with different extent of corrosion

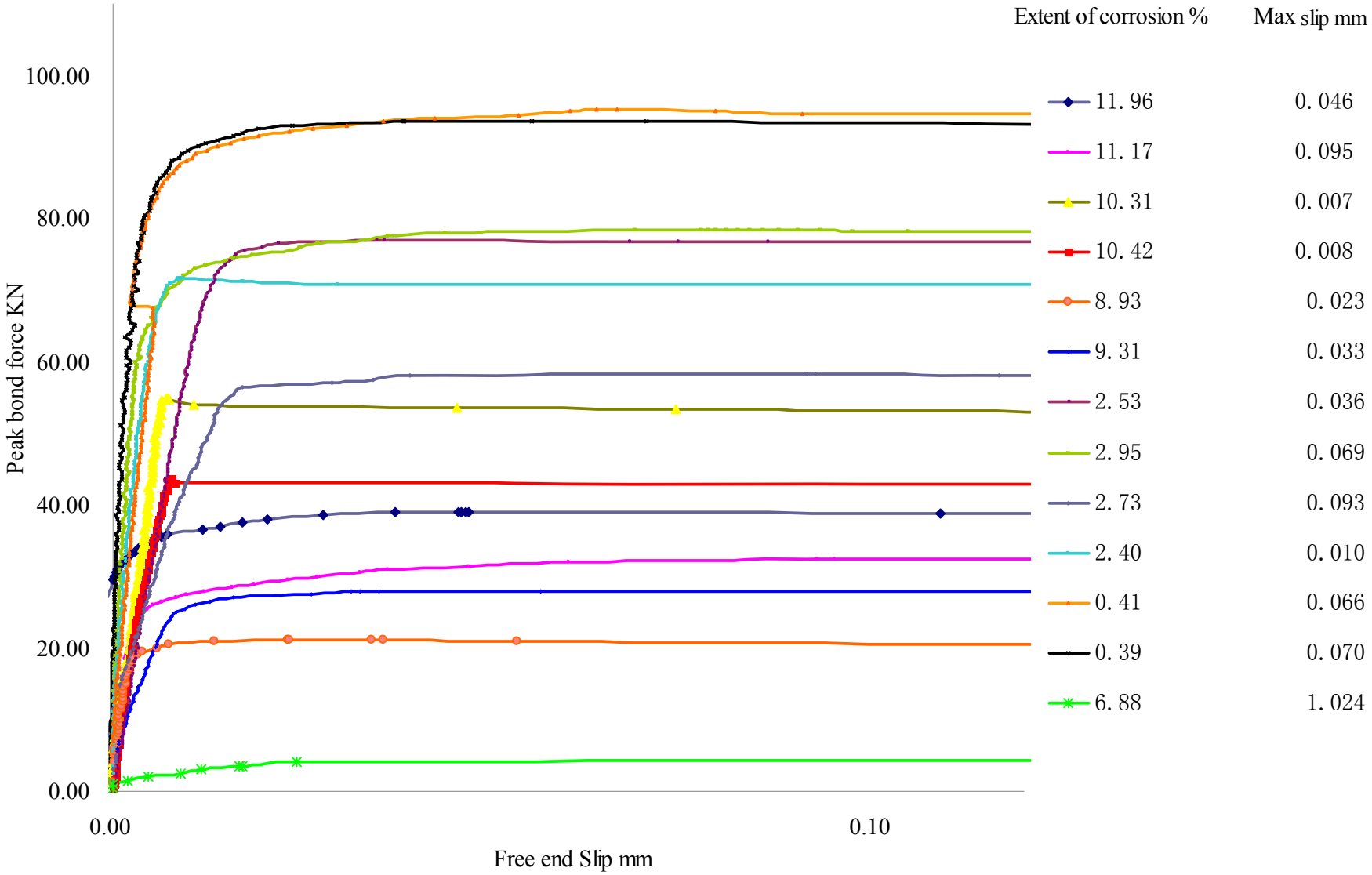

Figure 4.28 Peak bond force vs free end slip for 12 mm bars with 3 C/Φ with different extent of corrosion

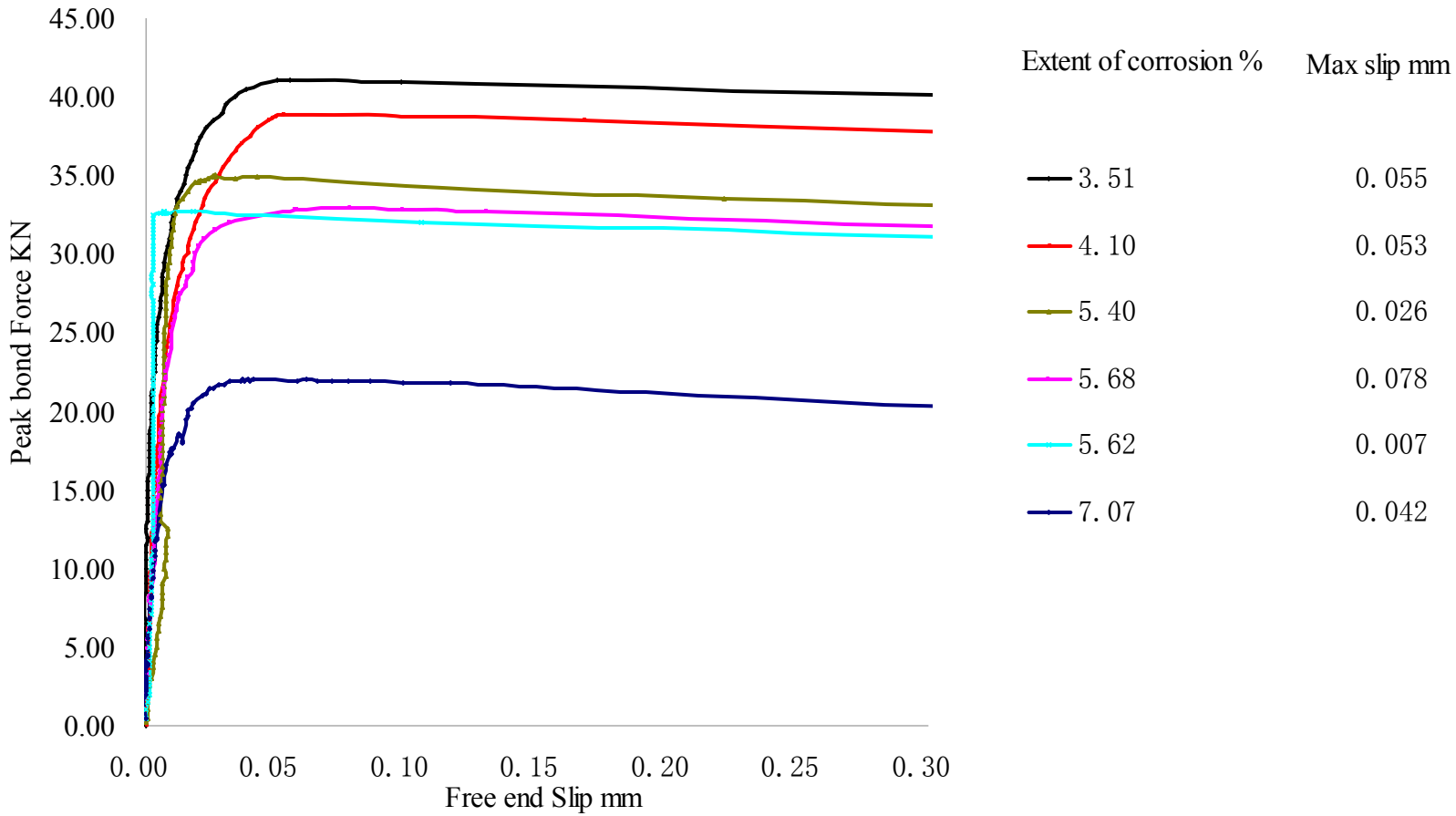

Figure 4.29 Peak bond force vs free end slip for 16 mm bars with 1 C/Φ with different extent of corrosion

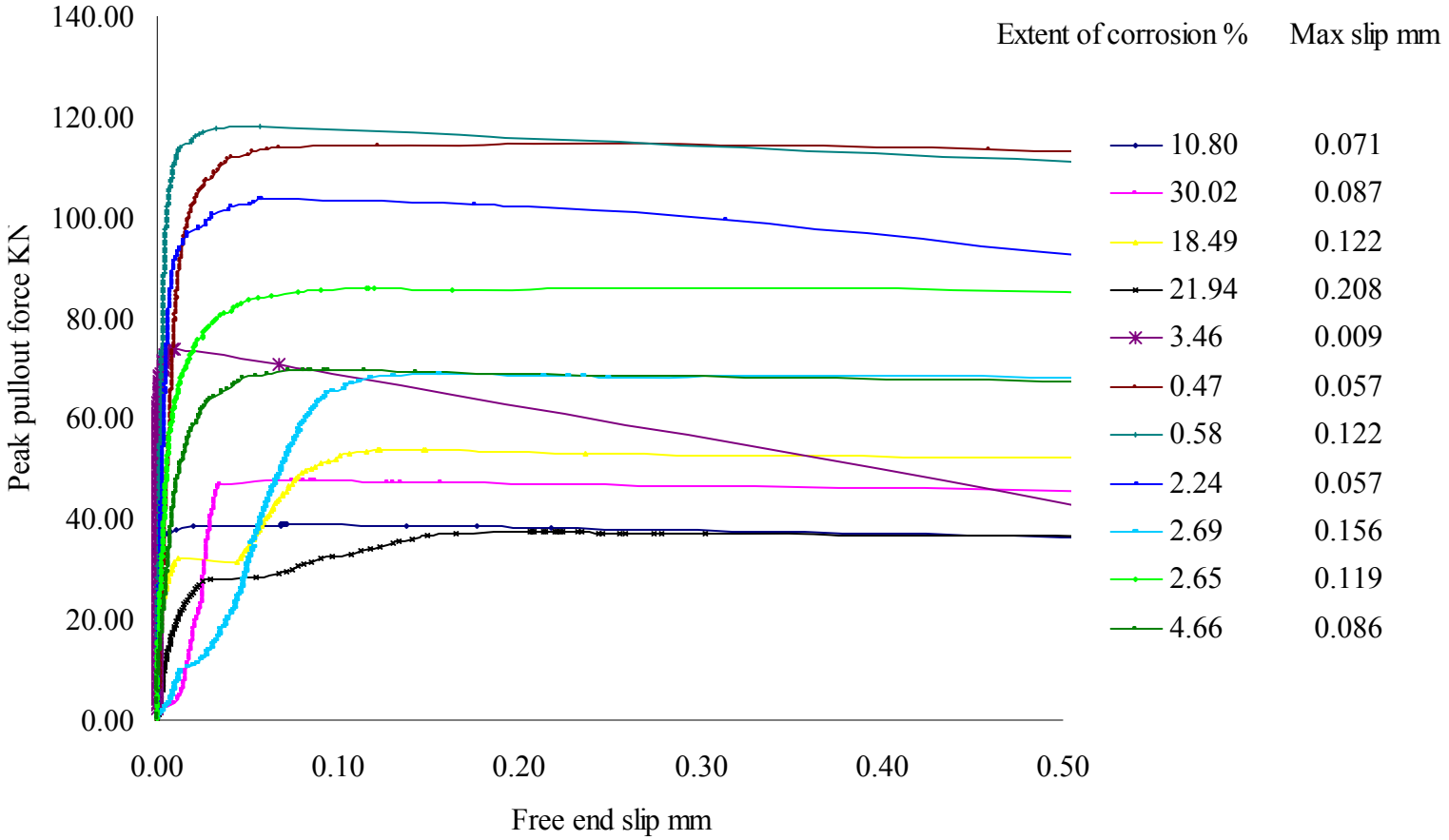

Figure 4.30 Peak bond force vs free end slip for 16 mm bars with 3 C/Φ with different extent of corrosion

The bond-slip results show no clear trends. Al-Sulaimani et al[23] have reported an increase of 'slip at ultimate bond stress' with increasing degree of corrosion. However, Auyeung et al [27] reported that corroded bars undergo reduced slip at peak bond stress as corrosion degree increases. Similar trends have been reported by Fang et al. [20] – ie slip at ultimate bond tended to decrease as the corrosion level increased.

4.6 Cracks pattern

Three stages to the cracking process were observed. The initial cracks occurred in a very short period, usually generated within several days. After that, most cracks grew gradually until they reached 1 mm. In the final stage, it was difficult to predict the crack width based on corrosion level, because it was difficult to ascertain the condition of the surrounding concrete. The results between corrosion level and crack width shows scatter indicating that it is not feasible to reliably relate the extent of corrosion and the crack width when the corrosion is above a certain degree. The results were found to diverge when the extent of corrosion is greater than 10%.

The first crack observed was a hairline crack with a width of approximately 0.05mm. This was termed crack initiation. These continuous longitudinal cracks appeared on the concrete surface parallel to the bars. Short unconnected longitudinal cracks were also occasionally observed parallel to the bars at lower corrosion levels.

Figures 4.31-4.36 show sketches of the different crack patterns observed in this study. For specimens with 1 C/Φ, the main longitudinal corrosion cracks appeared on vertical sides and with some of them appeared on the either the top or bottom surface (Figures 4.31-4.33). For specimens with 3C/Φ, all the main longitudinal cracks were observed level with the bars on the vertical sides of the specimens (Figure 4.31 and Figures 4.34-4.36). It also was observed that cracks progressed between two adjacent bars at higher corrosion levels (Figures 4.34-4.36)，and eventually connected. For some specimens, it was found that there were radial cracks inclined to the main cracks passing to another face.

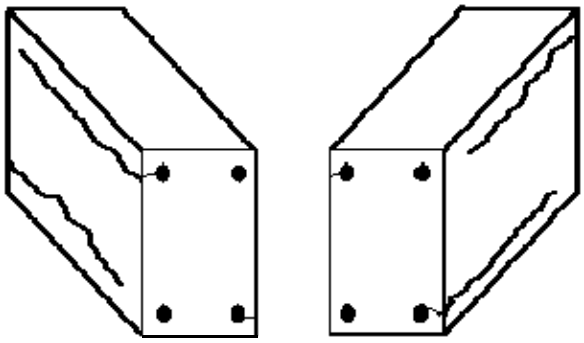

Figure 4.31 Type 1

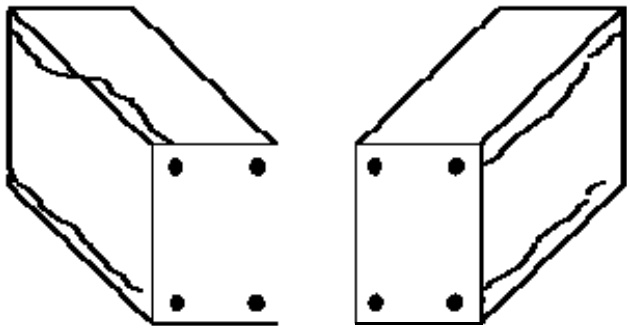

Figure 4.32 Type 2

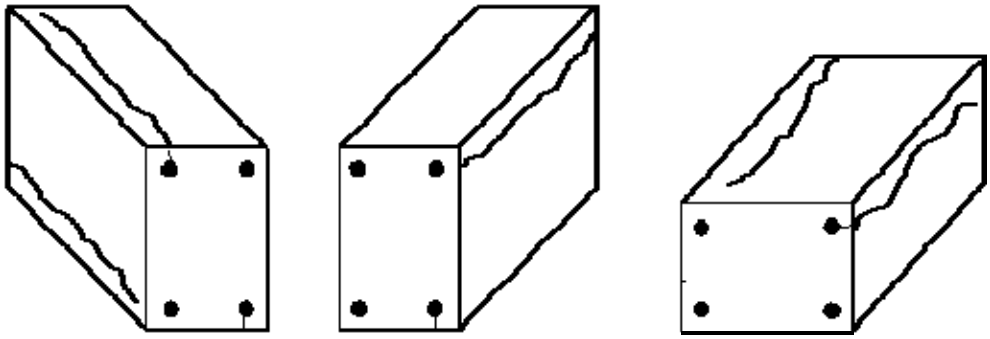

Figure 4.33 Type 3

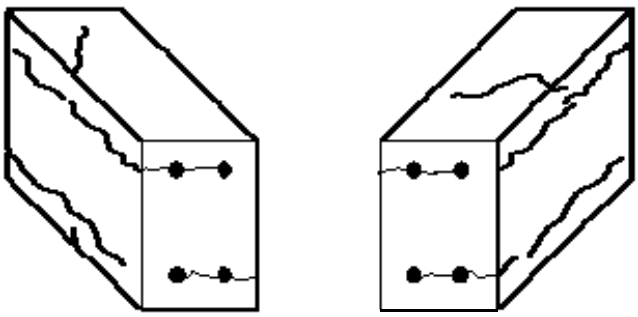

Figure 4.34 Type 4

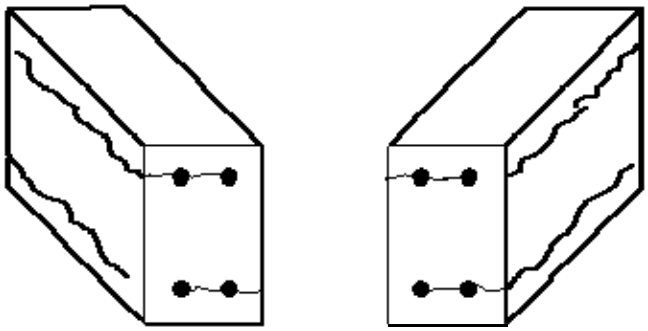

Figure 4.35 Type 5

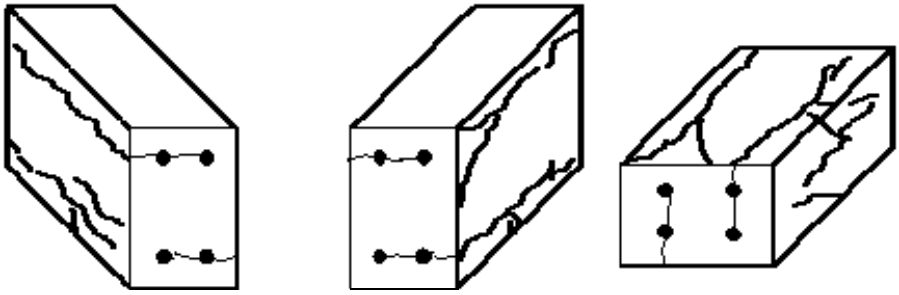

Figure 4.36 Type 6

Specification	Numbers of specimens	Type of Cracks pattern
12 mm, 1 C/Φ	3	2, 3
12 mm, 3 C/Φ	3	1, 4,5
16 mm, 1 C/Φ	4	1,2,3
16 mm, 3 C/Φ	7	1,3,4,5

Table 4.9 Summary of types of cracks pattern

Table 4.9 summaries the types of crack patterns on different the specimens.

5 Discussion

5.1 Effect of bar position

The effect of the bar position on the change of bond strength has been reported by many researchers. Higher bond strength has been reported on (non-corroded) bottom bars [41, 49] due to the superior quality of the steel-concrete interface. Defects caused by bleeding, settlement and segregation of fresh concrete under horizontal reinforcing bars can result in a decrease of bond strength in top bars. The top bars showed significant corrosion compared with bottom bars in work reported by Malhotra et al [18]. This supports the conclusion that concrete defects vary with bar position.

In this project, the effect of bar position was compared on corroded bars with minor corrosion levels (less than 1%). In Tables 4.5-4.8, the difference between top and bottom bars are reported for Φ16 mm bars with 1 C/Φ. Results for bottom cast bars were found to be 30% higher than those for top cast bars. For similar extent of corrosion on Φ12 mm bars with 1 C/Φ, the bond strength of bottom bars was 8% higher than top cast bars. However, for specimen with 3 C/Φ, there is little difference of bond strength due to this position effect. Indeed some individual bond strengths of top bars were found to be higher than bottom cast bars. This is probably due to the bars being further from the surface because of higher cover and hence surface zone effects become insignificant. When reinforcing bars were corroded to a extent of corrosion greater than 1%, the influence of bar position became negligible. This is probably because the properties of the steel/concrete interface had become similar for both top and bottom cast bars due to the expansion of the corrosion product, and other factors such as crack width having an increased effect.

5.2 Bar size effects

To analyse the effect of bar size on bond strength, the results for controlled specimens (non-cracked specimens) with similar extent of corrosion were used (Table 5.1)

Specification	Bond strength (N/mm^2)	
	Top	Bottom
12 mm, 1C/Φ	3.09	3.617
	3.50	3.499
16 mm, 1C/Φ	2.95	3.224
	1.78	3.101
12 mm, 3C/Φ	8.43	8.286
	7.70	7.838
16 mm, 3C/Φ	8.06	7.531
	7.591	7.835

Table 5.1 Bond strength of non-cracked specimens

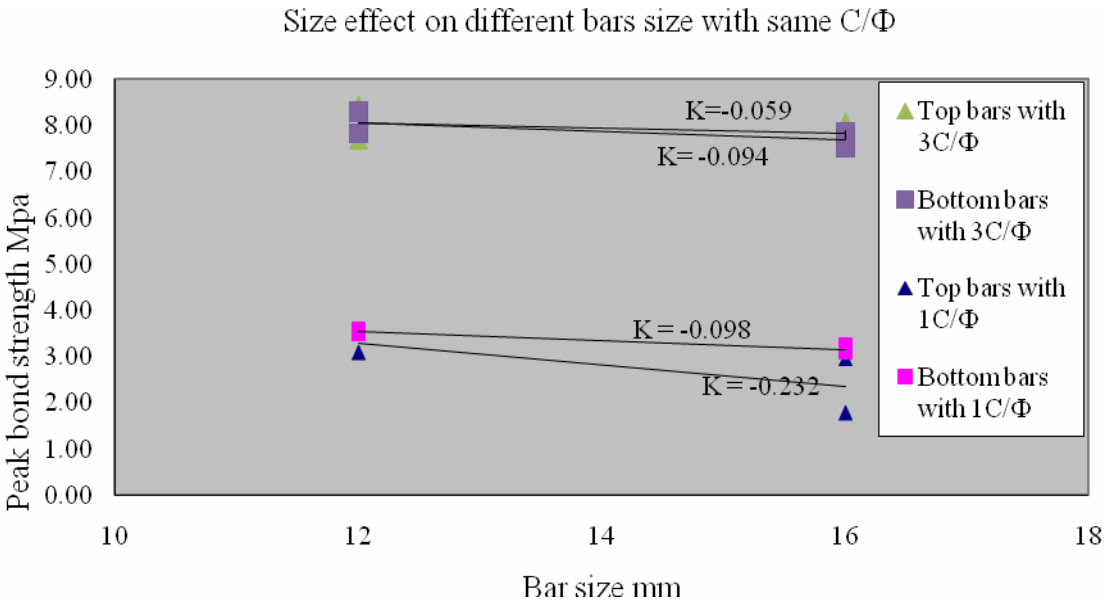

Figure 5.1 Bar size effect on specimens with the same C/Φ

Figure 5.1 clearly shows a size effect for the bond strength of bars with equal C/Φ. The 12 mm bars have a higher peak bond strength than the 16 mm bars with the same C/Φ. The slope of the line, K, is the measure of the effect of bar size on the bond strength. However, considering the scatter of the results, a large numbers of specimens need to be tested to accurately determine the magnitude of this factor.

The K values indicate that the influence of the size-effect on bond strength becomes smaller

as the cover/diameter ratio increases. That is, pull-out specimens with smaller cover exhibit a larger size-effect, which may be attributable to brittle splitting cracks. A similar trend has been reported by Ichinose [44]. However, for corroded bars, it is difficult to compare the size effect because of scattered results due to different levels of corrosion.

5.3 Effect of concrete strength on bond strength

Batches of specimens for 16 mm bars with different compressive strength have been used to compare the effect of concrete strength on the bond strength. In order to compare bond strength for the different concrete compressive strengths, Equation 5.1 is used to normalize bond strength for non-corroded specimens as has been used by other researcher [45].

$$\tau' = \tau_{exptl}\sqrt{\frac{40}{f_c}} \qquad 5.1$$

Where τ' is bond strength for grade 40 concrete, τ_{exptl} is the experimental bond strength and f_c is the experimental compressive strength.

The bond stress is compared on the basis of the similar extent of corrosion for controlled specimens (no-cracked) in Table 5.2.

The results indicate that the bond stress tends to increase with the increase of concrete compressive strength at low corrosion level. However, there is no clear trend that it has a direct relationship with the square root of the compressive strength.

16 mm Bars	Bar position	compressive strength (MPa)	Bond strength (N/mm^2)	Normalized bond stress (N/mm2)	Extent of corrosion (%)
1C/Φ	T	37.5	2.951	3.048	0.44
	T		1.780	1.838	0.37
	B		3.224	3.330	0.39
	B		3.101	3.203	0.32
	T	50	2.524	2.258	0.19
	T		2.188	1.957	0.18
	B		4.313	3.858	0.15
	B		3.560	3.184	0.20
3C/Φ	T	40	8.062	8.062	1.29
	B		7.531	7.531	1.13
	T	42.5	7.591	7.364	0.58
	B		7.835	7.601	0.47
	T	50.5	6.870	6.114	0.31
	B		8.038	7.154	0.62

Table 5.2 Normalised bond strength

5.4 Effect of crack width and extent of corrosion on bond strength loss

Figures 5.2-5.13 (from the results of Tables 4.5-4.8) show the relationship between bond strength with the change of crack width and the extent of corrosion.

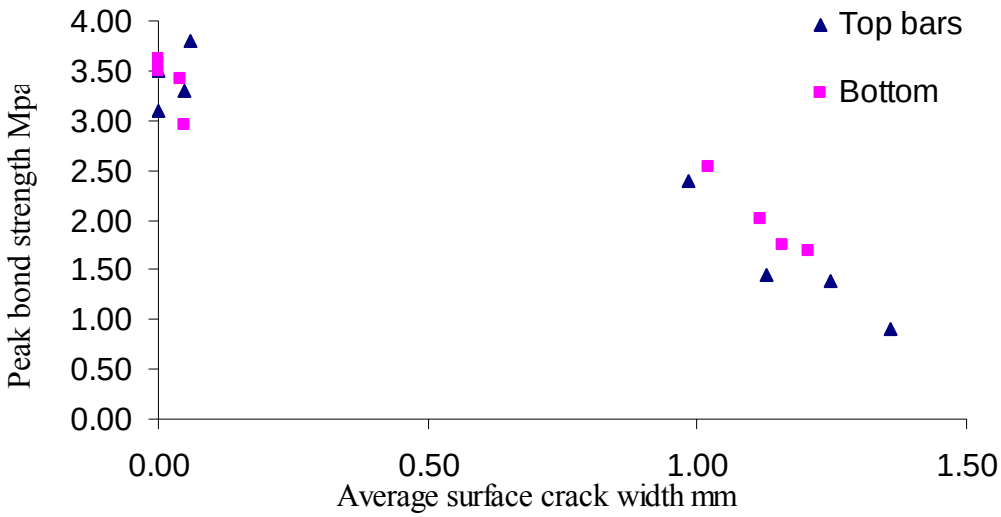

Figure 5.2 Peak bond strength vs average surface crack width for 12 mm bars with 1 C/Φ

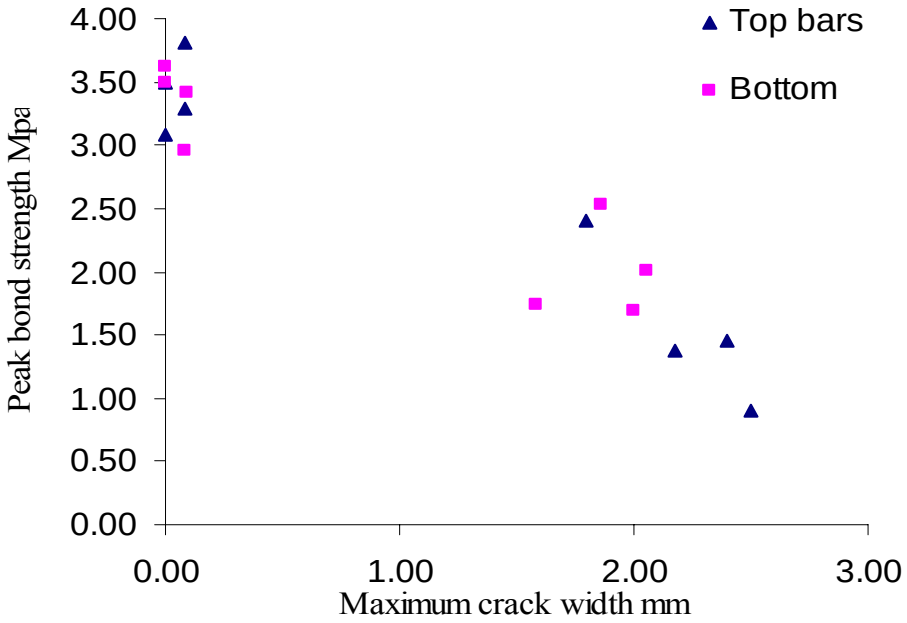

Figure 5.3 Peak bond strength vs maximum surface crack width for 12 mm bars with 1 C/Φ

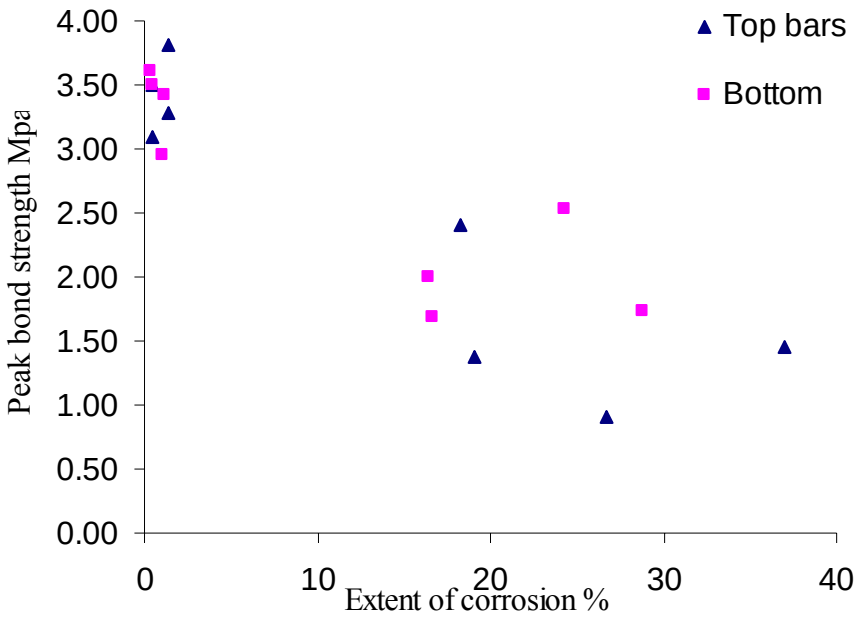

Figure 5.4 Peak bond strength vs extent of corrosion for 12 mm bars with 1 C/Φ

For 12 mm bars with a cover of one diameter, the bond strength remains almost constant up to the appearance of the first visible crack (0.05mm). This first crack corresponded to a corrosion level less than 1.35%. The bond strength then decreases significantly at crack width of 1mm and above. For crack widths of 1mm, the bond strength has reduced by 27% and 29% for top and bottom bars respectively. However, for higher corrosion levels, the bond strength is more scattered. Comparing Figures 5.2-5.4, the bond strength shows the best relationship for peak bond strength against average crack width rather than peak bond strength against extent of corrosion. Bond strength increased at initial cracking for bars with 1 C/Φ and dropped for bars with 3 C/Φ- this has been discussed in Section 5.5.

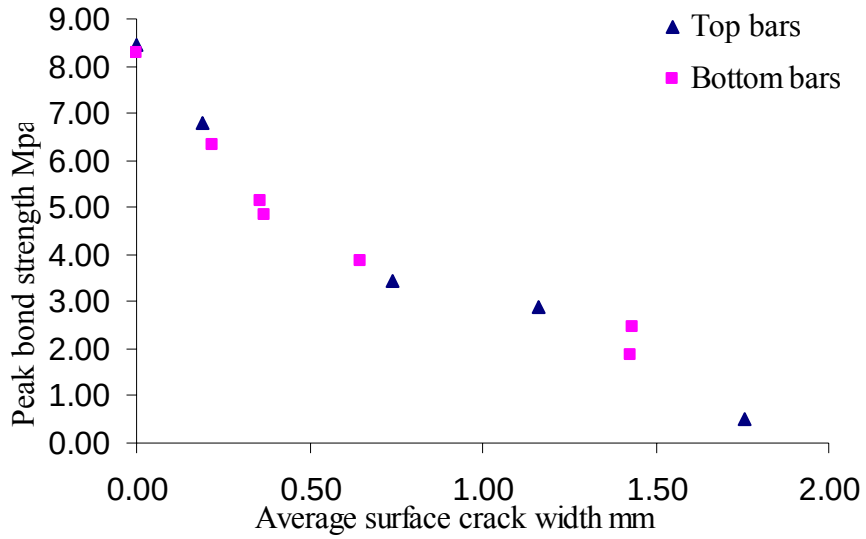

Figure 5.5 Peak bond strength vs average surface crack width for 12 mm bars with 3 C/Φ

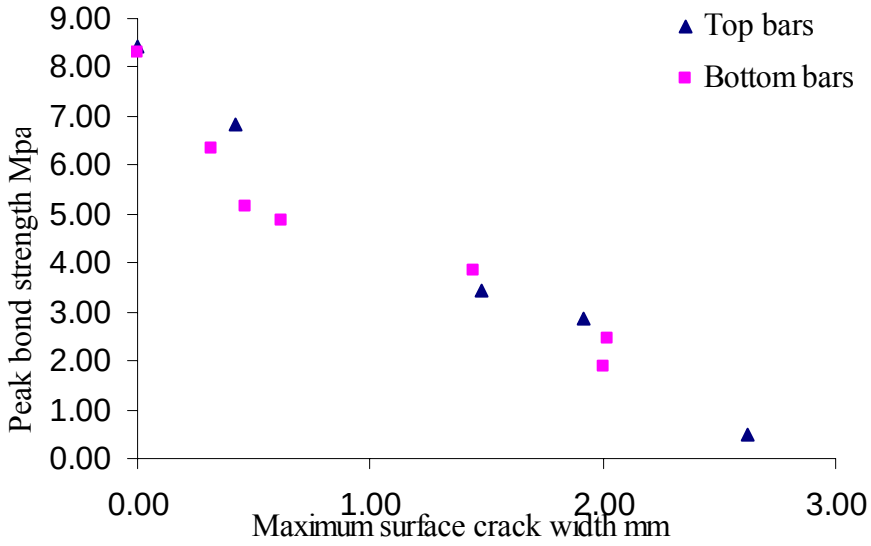

Figure 5.6 Peak bond strength vs maximum surface crack width for 12 mm bars with 3 C/Φ

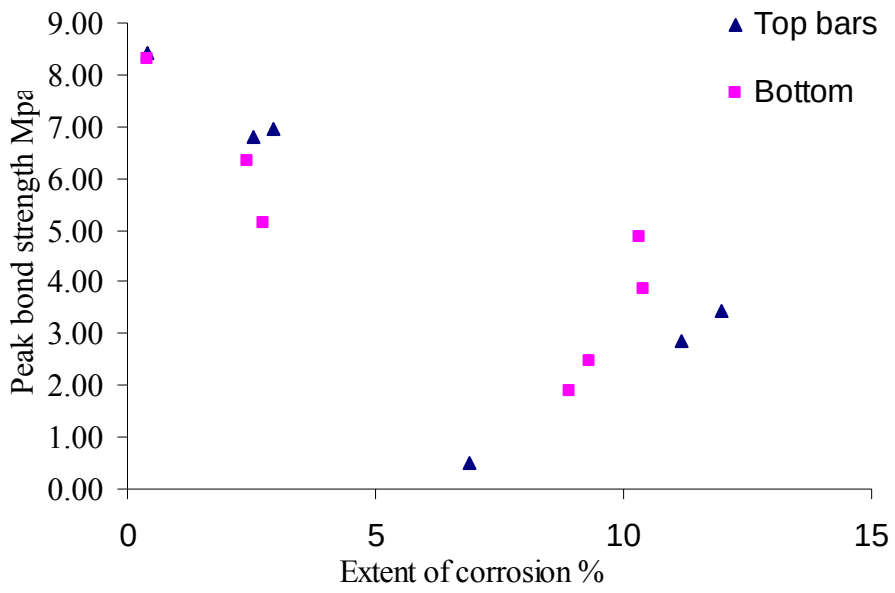

Figure 5.7 Peak bond strength vs extent of corrosion for 12 mm bars with 3 C/Φ

By comparing Figures 5.5-5.7 for 12 mm bars with 3 C/Φ, a clear trend for bond strength and average crack width is observed. The bond strength drops gradually with an increase of average surface crack width and maximum crack width. The bond strength is seen to reduce by 19% and 38% for top and bottom bars respectively at crack widths of approximately 0.5mm. However, results are more scattered in Figure 5.7 for higher corroded bars with corrosion levels around 10%.

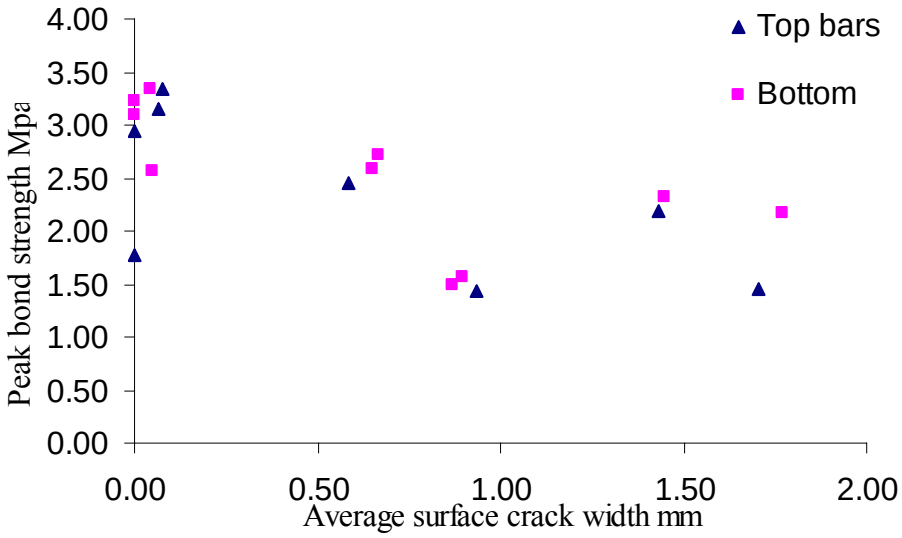

Figure 5.8 Peak bond strength vs average surface crack width for 16 mm bars with 1 C/Φ

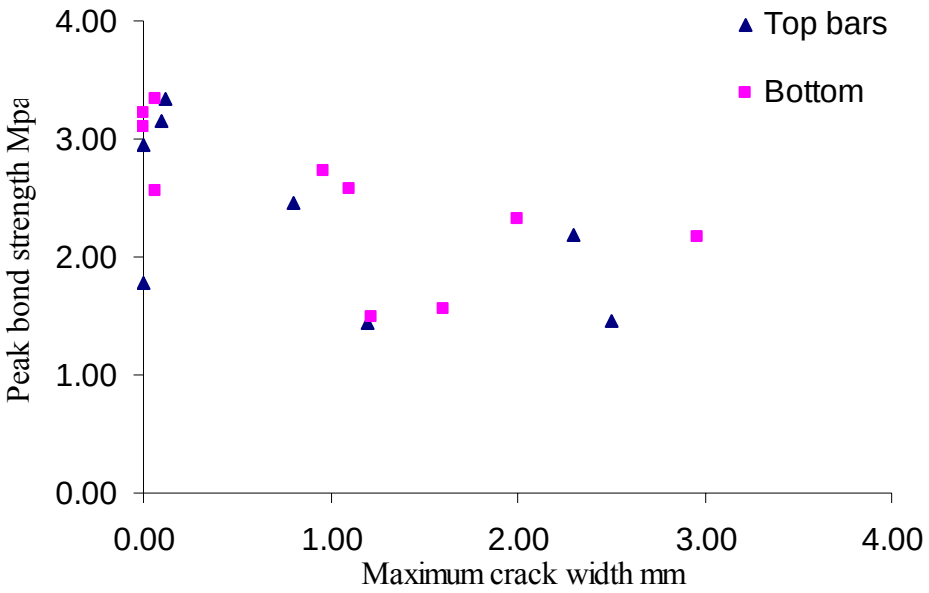

Figure 5.9 Peak bond strength vs maximum surface crack width for 16 mm bars with 1 C/Φ

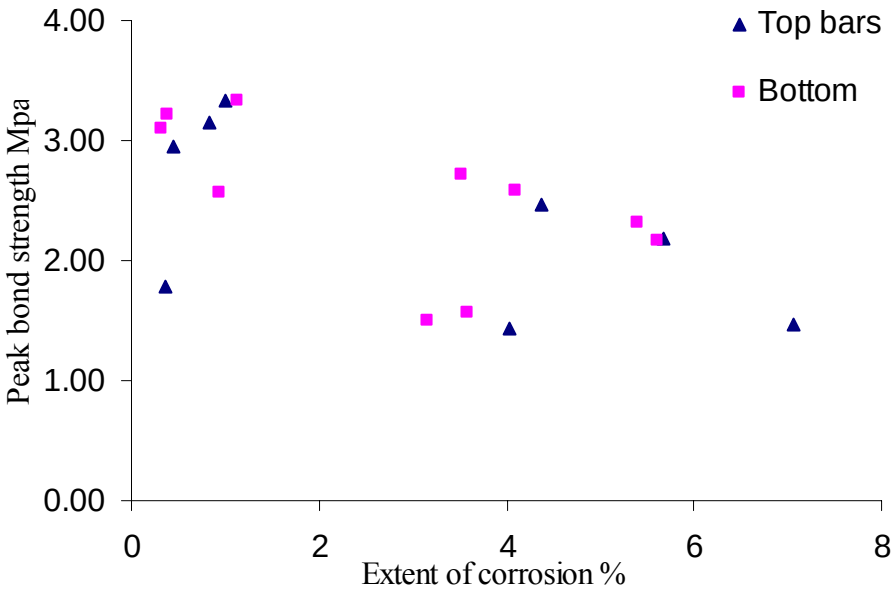

Figure 5.10 Peak bond strength vs extent of corrosion for 16 mm bars with 1 C/Φ

Figures 5.8-5.10 present the loss of bond strength with the change of cracks width and corrosion level for 16 mm bars with 1 C/Φ. Both Figure 5.8 and Figure 5.9 show a trend of decreasing bond strength although there is spread of results for cracks over 1 mm. A slight increase of bond strength for low corrosion levels (less than 2%) is observed in Figure 5.8 for top bars with relative crack width of 0.05 mm. The bond strength of both top and bottom bars have reduced by 51% at crack widths of 0.9 mm with corresponding corrosion levels of 3.5%.

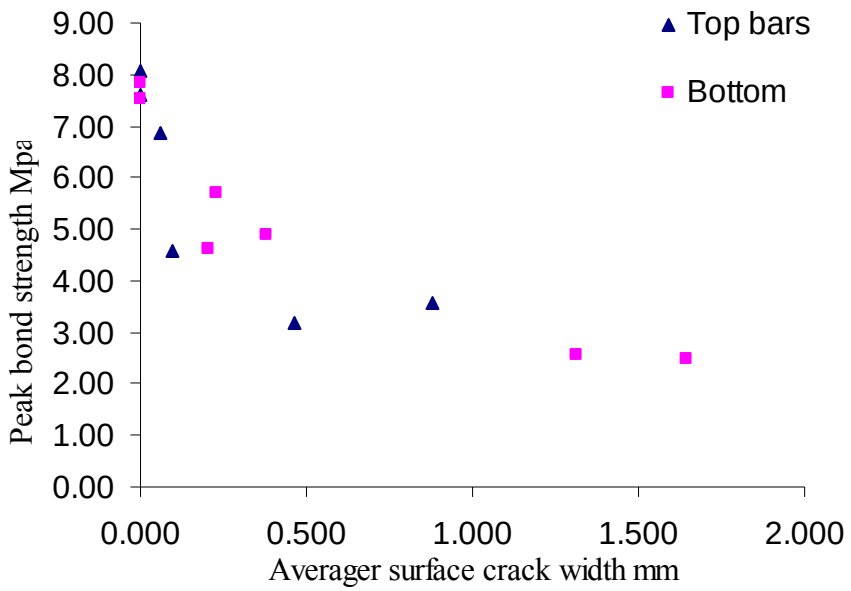

Figure 5.11 Peak bond strength vs average surface crack width for 16 mm bars with 3 C/Φ

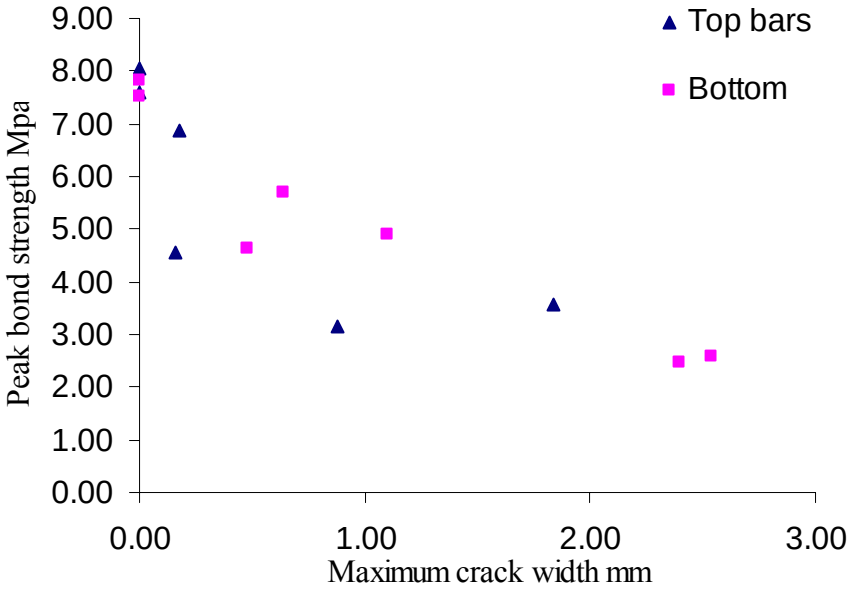

Figure 5.12 Peak bond strength vs maximum surface crack width for 16 mm bars with 3 C/Φ

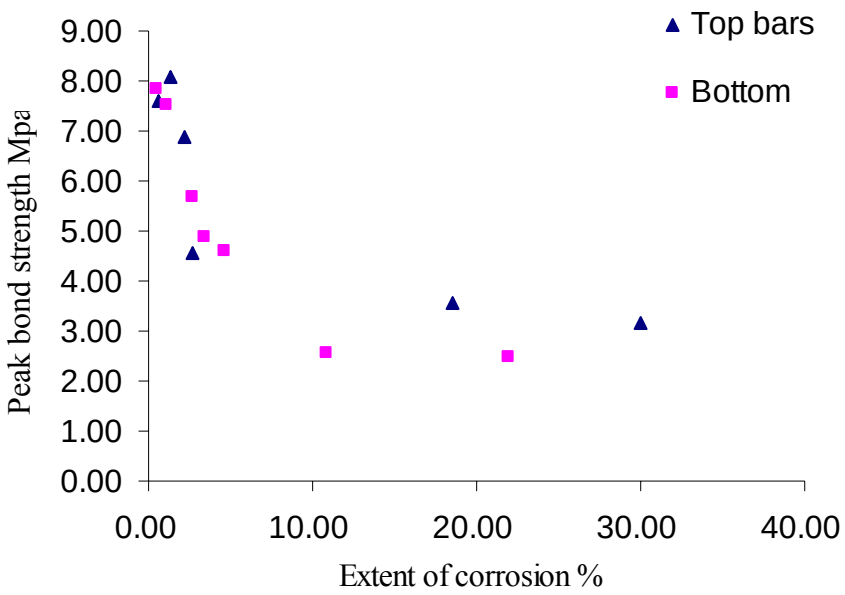

Figure 5.13 Peak bond strength vs extent of corrosion for 16 mm bars with 3 C/Φ

Results for 16 mm bars with 3 C/Φ were plotted in Figures 5.11-5.13. Again, a clear trend was found in both Figures 5.11 and 5.13. For top bars, the bond strength has reduced by 12% at crack widths of 0.06 mm with a corresponding corrosion level of 2.24% for top bars. It then is seen to drop to 60% at a crack width of 0.5 mm with a corresponding corrosion level of 30%. For bottom bars, the bond strength decreased by 36.4% at a crack width of 0.38 mm with only 3.46% mass loss. The 32% residual bond strength remained when the crack width reach up 1.6 mm at higher corrosion levels (21.9%).

Comparing Figures 5.2-5.7, the conclusion can be drawn that bond strength has a better relationship with average surface crack width for 12 mm bars. For 16 mm bar with 1 C/Φ (Figure 5.8), it shows a clear trend for cracks width under 1 mm, although results become scattered at larger crack widths. Although there is a trend for 16 mm with 3 C/Φ (Figure 5.13), it can be seen that there is a spread of results at the higher corrosion level (over 10%). The effect of crack width on bond strength loss can be explained as loss of confinement. Research by Cairns et al. [50] shows that corrosion products do not impair friction characteristics of a bar/concrete interface where the surface crack width does not exceed 1.0 mm indicating that extent of corrosion has less effect on the change of bond strength.

5.5 Influence of C/Φ ratio

The generally accepted concept of the change of bond strength with corrosion is that the bond strength will increase before corrosion induced cracking is observed. Figures 5.2-5.4 show

that the bond strength for 12 mm bars with 1 C/Φ initially increases for top bars, and remains constant for bottom bars when the first initial cracks occur. For 16 mm bars with 1C/Φ (Figure 5.8), both top and bottom bars show an increase of bond strength at initial cracking. However, for 16 mm bars with 3 C/Φ (Figure 5.11), the bond strength reduces at the initial cracking stage. The difference is probably because of the different range of corrosion level required for initial cracking for different C/Φ. It was found that approximately 1% mass loss was required for initial cracking for bars with 1 C/Φ, while 2.5% mass loss was needed for initial cracking for bars with 3 C/Φ. Another reason is probably due to the quality of the surrounding concrete. For bars with 1 C/Φ, the composition of the concrete around the bar may be less homogeneous than for bars with 3 C/Φ (as discussed in Section 5.1).

For cracks greater than 1.0 mm, the bond strength has a similar residual strength for 16 mm bars for the range of C/Φ tested. The bond strength decreased more sharply for 3 C/Φ than for 1 C/Φ at similar crack widths. Again, this would indicate that with the increase of cover/diameter ratio, the effect of crack width becomes more pronounced. The appearance of cracking was observed after a longer time period for larger covers.

5.6 Extent of corrosion vs crack width

Studies on corrosion cracks have been reported by many researchers. Several have found that there is a weak relationship between crack width and corrosion rates [7, 51]. However, others conclude that there is no relationship between crack width and corrosion rates [4, 29, 30]. Research by Mohammed [28] reported that the crack widths were observed to correlate with corrosion rate at the very beginning of the exposure period only. Consequently there is no accepted clear relationship between corrosion level and crack width. This is probably due to non-uniform corrosion at the bar surface. Localized corrosion affects extent of corrosion significantly, however, it has less effect on the average crack width. Another possibility is that once surface cracks occur, the growth of the surface crack width is not fully dependent on the growth of corrosion product due to other cracks occurring inside the concrete.

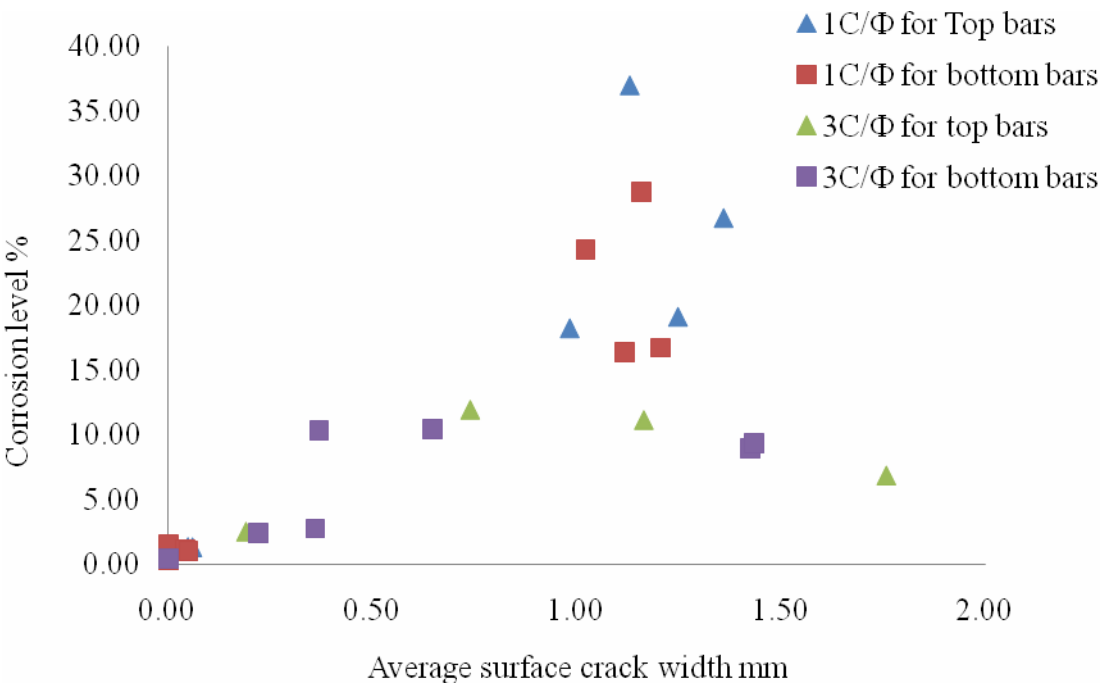

Figure 5.14 Crack width vs corrosion level for 12 mm bars

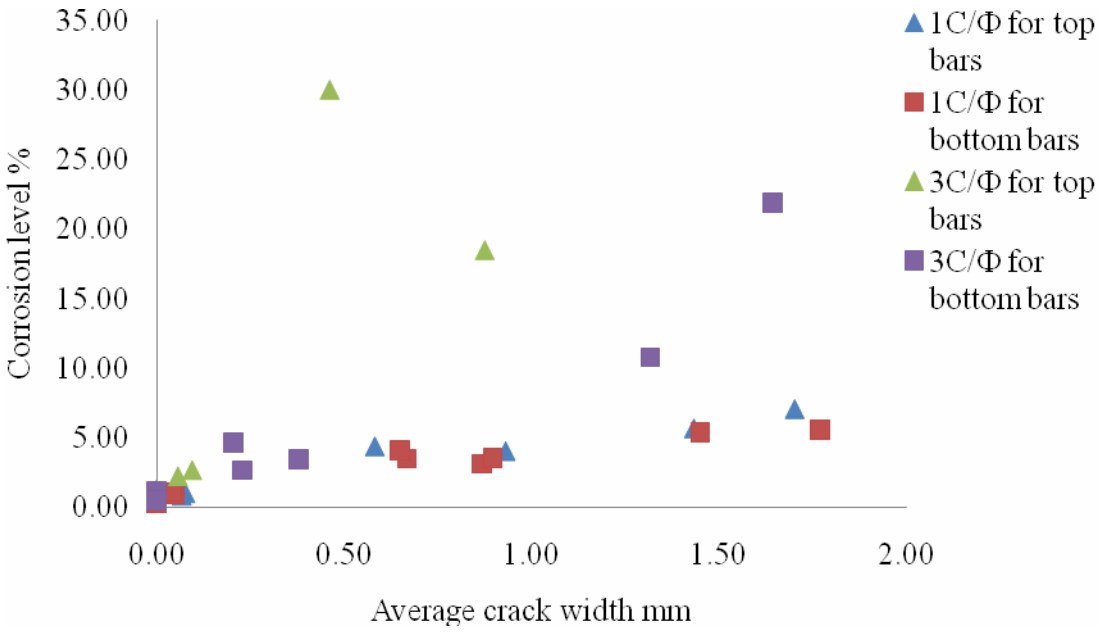

Figure 5.15 Crack width vs corrosion level for 16 mm bars

Figures 5.14-5.15 show the average surface crack width versus change of corrosion level. Although there is a trend, it can be seen that there is a spread of results at the greater crack widths (Figure 5.14). Similar behaviour was observed by Alonso et al [1]and Vidal et al [3]. This can be explained due to localized corrosion having less effect on corrosion cracking.

Figure 5.15 shows, for 16 mm bars, that a higher corrosion level was required for larger C/Φ to achieve a similar crack width. Corresponding data for 12 mm bars is inconclusive and additional data would be required to determine if similar trends occur.

In several cases, it was observed that initial crack width increased at a steady (near constant) (time) rate up to a point (at approximately 1mm or even larger), after this point the rate of crack width growth increased dramatically. This suggests that initially the crack width is related to the volume of corrosion product, but after a critical width is reached, concrete spalling occurs.

5.7 Effect of impressed current

It has been reported by others [2, 9] that extent of cracking will be affected by the impressed current. Consequently, whilst the results from accelerated corrosion tests provide reliable relative data, the quantitative relationship between cracking as a result of accelerated and natural corrosion needs further investigation if these results are to be used in the field.

Data in Table 5.3 is presented to assess the effect of impressed current on crack width and bond strength (see Table 4.5) for specimens with 12 mm bars with 1C/Φ. This table shows results for a specimen (marked *) that was left for approximately one year without impressed current and achieved a level of corrosion greater than that which would have caused cracking had it been accelerated.

The results show that for a similar extent of corrosion, the accelerated specimens had already cracked, while the specimens under natural corrosion exhibited no cracks. The data indicates that the impressed current does have an effect on crack growth. The relationship between bond strength and crack width for both accelerated and non-accelerated specimens is similar. Considering the higher scatter of the results, it appears that using crack width as a means of assessing residual bond strength is more reliable than using extent of corrosion.

Specification	Bar Position	Average Surface crack width (mm)	Bond Strength (N/mm^2)	Extent of corrosin (%)
Accelerated specimens	T	0.000	3.087	0.52
	T	0.000	3.5	0.42
	T	0.048	3.289	1.35
	T	0.059	3.806	1.33
	B	0.000	3.617	0.33
	B	0.000	3.499	0.46
	B	0.042	3.421	1.19
	B	0.049	2.956	1.07
Natural corrosion *	T	0	4.017	1.47
	T	0	3.646	1.25
	B	0	4.279	1.29
	B	0	3.13	1.52

Table 5.3 Results of specimens under accelerated and natural corrosion

The above results and discussion from Sections 5.6 and 5.7 show that the critical corrosion level to cause concrete cracking is dependant on the cover depth, corrosion rate and diameter of the reinforcing steel. This conclusion is also drawn in other research [52]. It is possible to relate the crack width and corrosion level at initial stages of corrosion. However, no clear relationship between extent of corrosion with crack width has been found at higher corrosion levels in this study.

5.8 Characteristics of corroded steel bars

5.8.1 Bond stress development length

AS 3006 [53] gives Equation 5.2 for the development length to develop yield strength;

$$L_{sy.t} = \frac{k_1 k_2 f_{sy} A_b}{(2a + d_b)\sqrt{f_c'}} \geq 25 K_1 d_b \qquad 5.2$$

Where

k_1 = 1.25 for a horizontal bar with more than 300mm of concrete cast below the bar; or
= 1.0 for all other bars

k_2 = 1.7 for bars in slabs and walls if the clear distance between adjacent parallel bars developing stress is not less than 150mm;
= 2.2 for longitudinal bars in beams and columns with fitments;
= 2.4 for any other longitudinal bar

A_b = cross-sectional area of the reinforcing bar.

2a = twice the cover to the deformed bar or the clear distance between adjacent parallel bars developing stress, whichever is less.

Values of $L_{st,t}$ for 12 mm bars with 1 C/Φ and 3 C/Φ are 596 mm and 199 mm respectively. The corresponding values for 16 mm bars are 830 mm and 277 mm. When comparing the embedded length of the specimens used in this project (300 mm) with these values, it shows that the anchorage lengths are equal or less than the development lengths. Kayyali et al [54] concluded that the calculated value for the bond strength reduces when the anchorage length exceeds the development level. Therefore, the effect of tensile failure of the steel has not been considered when assessing the bond strength. It can be predicted that the effect of corrosion on the change of cross section will reduce the bond development length given by Equation 5.2.

5.8.2 Rupture of steel bars during pullout test

The rupture of the reinforcement was observed on two 16 mm corroded bars in specimens with 3 C/Φ. These corresponded to a pullout test at 60.01 KN and 40.73 KN with the related crack width 0.58 mm and 0.55 mm respectively. The bar at 60.01 KN has corrosion level of 30.6%. This would indicate a large section loss on the bar due to localized corrosion.

Figures 5.16-5.17 show the typical bond-slip curve for the loaded end and free end.

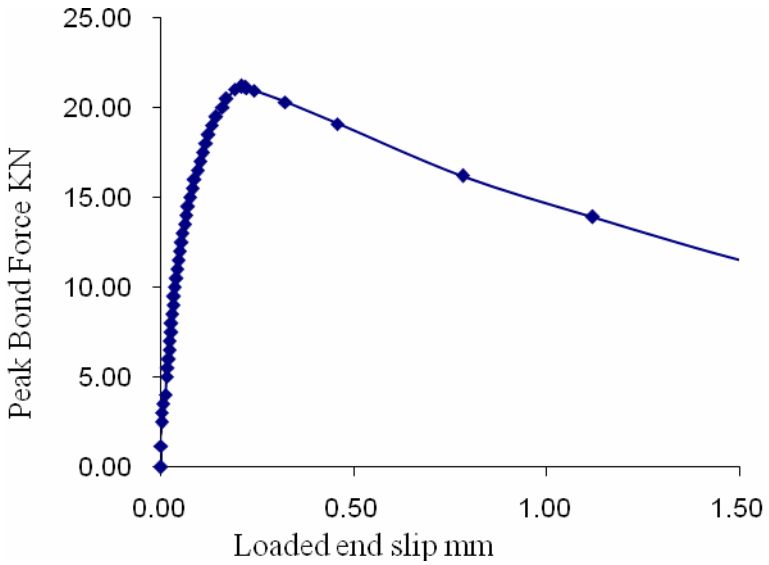

Figure 5.16 Peak bond force vs loaded end slip

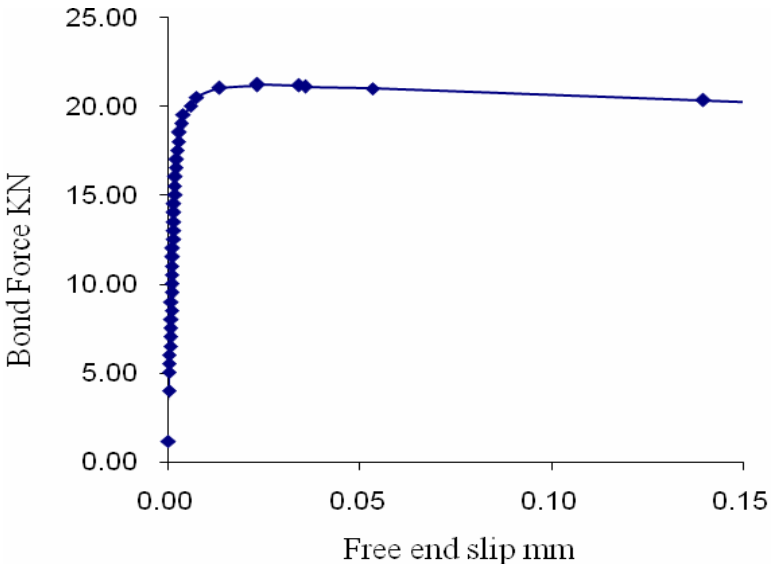

Figure 5.17 Peak bond force vs free end slip

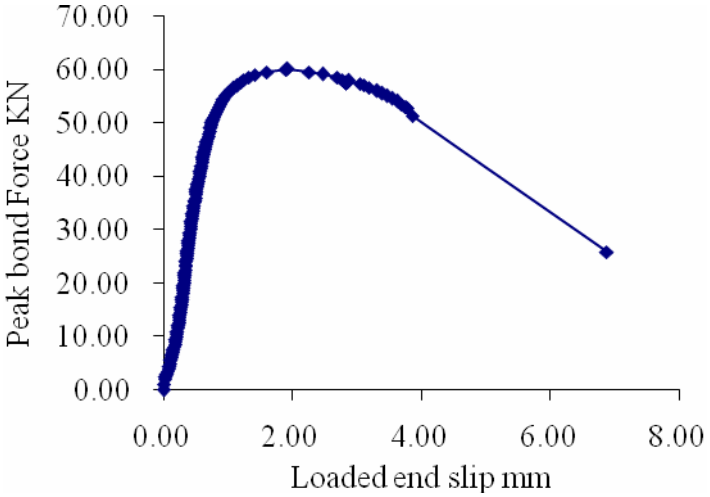

Figure 5.18 Peak bond force vs loaded end slip

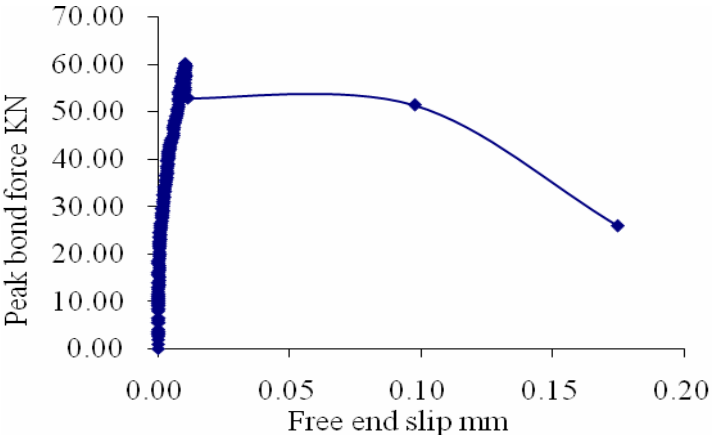

Figure 5.19 Peak bond force vs free end slip

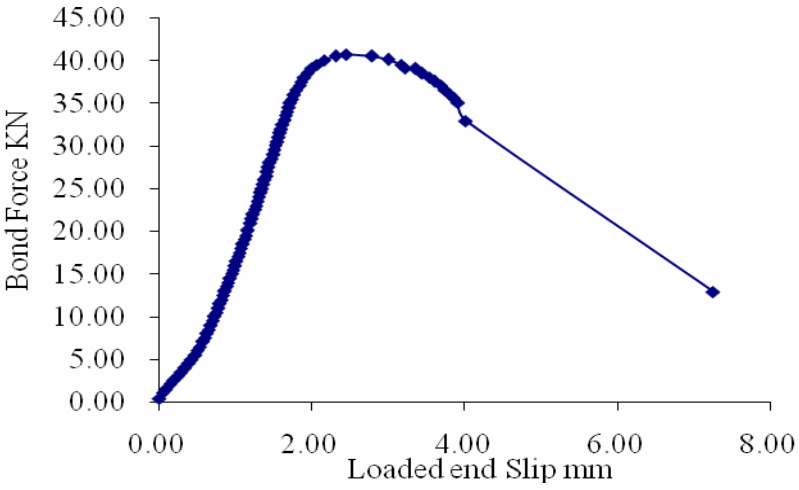

Figure 5.20 Peak bond force vs loaded end slip

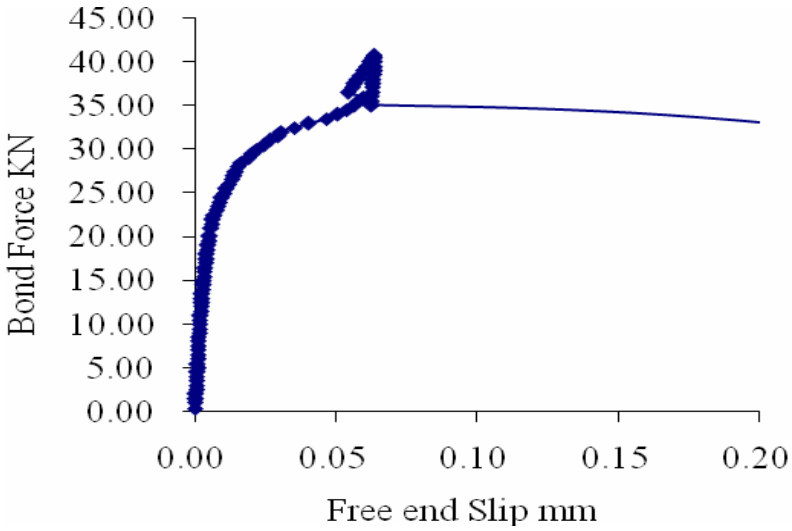

Figure 5.21 Peak bond force vs free end slip

Figures 5.18-5.21 show the peak bond force vs loaded end slip and free end slip on the ruptured bars. Comparing the curve of bond vs loaded end slip, the variation in trend for higher bond values is believed to be due to the yield of the corroded bars. It was observed that the bond stress decreased dramatically without change of free end slip when the reinforcement reached the yield plateau. The free end slip was in some cases seen to reverse at peak load (Figure 5.21). This was due to elastic energy stored in the support system resulting in the bar still moving after peak load. Failure of bar itself instead of bond suggests that the localized corrosion seriously inhibited the bar ductility. For localized corrosion, the investigation of section loss is important to assess the residual bond strength. However, it again suggests that crack width is an important parameter to correlate to the bond strength if the section loss of the steel bars is within a certain range.

Figure 5.22 derived from the discussion above shows how homogenous corrosion and localized corrosion work together on the structure. It can be seen that with both homogenous and localised corrosion, the dominating factor for structural safety with regard to corrosion is the extent of the different types of corrosion.

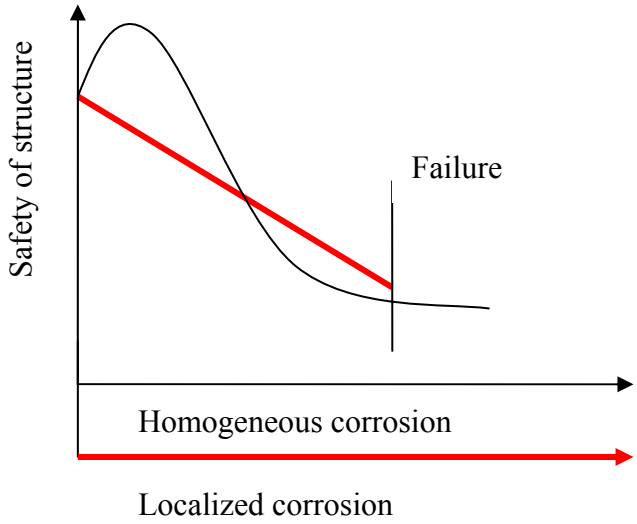

Figure 5.22 Combined effect of localized corrosion and homogeneous corrosion on structural safety.

6 Conclusions and Recommendations

Based on the results reported in this thesis and observations during the experimental investigation, the following conclusions can be drawn:

1. On non-cracked specimens, with a cover of 1 C/Φ, 16 mm bars exhibit a higher influence of bar position on bond strength than 12 mm bars. However, for bars with a cover of 3 C/Φ, the effect of bar position on bond strength becomes negligible. This is attributed to the higher cover reducing the influence of variation of surface zone concrete homogeneity. When reinforcing bars are corroded in excess of 1%, the influence of bar position becomes negligible.

2. For bars with equal C/Φ, 12 mm bars show higher peak bond strength than 16 mm bars. This size-effect on bond strength reduces with an increase of cover/diameter ratio.

3. There is no clear evidence that bond strength has a direct relationship with the square root of the compressive strength for uncracked sections.

4. The data indicates that there is a relationship between bond strength and average surface crack width. This is clearly evident for specimens with 12 mm bars with 1 C/Φ and 3 C/Φ at all crack widths. For specimens with 16 mm bars with 1 C/Φ, the relationship is less apparant at crack width greater than 1 mm.

5. The relationship between crack width and bond strength becomes more pronounced with the increase of cover/diameter ratio. The crack appearance is delayed (requiring greater corrosion) for larger covers. Cover/diameter ratio should be taken into account when using crack width to assess bond strength loss.

6. The bond strength has a better relationship with the surface crack width than the corrosion level. This is probably because once cracks reach a certain width; corrosion has less impact on crack progression.

7. The corrosion level required to initiate cracking is dependent on the cover depth, corrosion rate and size of the reinforcing steel. Use of an impressed current has an effect on crack growth. This indicates that using crack width as a parameter to assess residual bond strength

is more reliable than using the corrosion level.

8. Pullout tests on unconfined 12 mm bars with a cover of one diameter show no loss of bond strength at first visible external crack. The bond strength has a substantial loss (of approximately 50%), when the crack width reaches 1 mm.

9. Surface crack width may be a viable parameter to assess residual bond strength.

Recommendations for the future work

It should be noted that all conclusions drawn in this project are based on tests on unconfined specimens, accelerated by impressed current. The following recommendations are made for future research.

1. Specimens with stirrups should to be tested to see if there is still a relationship between bond loss and surface crack width.
2. Bond strength at similar crack widths should be compared for specimens with natural and accelerated corrosion.
3. Further test should be undertaken on specimens with crack width less than 1 mm and with a extent of corrosion less than 15%.
4. Computer based imaging technology should be assessed as a method to quantify the surface crack width in order to provide more accurate crack width measurements, to allow assessment of crack area and to save time.

7 References

1. Alonso, C., et al., *Fators controlling cracking of concrete affected by reinforcement corrosion.* Materials and Structures, 1998. **31**: p. 435-441.
2. Andrade, C., et al., *Cover cracking and amount of rebar conrrosion: importance of the current applied accelerated tests.* Concrete Repair, Rhabilitation and Protection, 1996.
3. Vidal, T., A. Castel, and R. Francois, *Analyzing crack width to predict corrosion in reinforced concrete.* Cement and Concrete Research, 2004. **34**(1): p. 165-174.
4. Arya, C. and F.K. Ofori-Darko, *Influence of crack frequency on reinforcement corrosion in concrete.* Cement and concrete composites, 1996. **26**(3): p. 345-353.
5. Maaddawy, E.T., K. Soudki, and T. Topper, *Long-term Performance of Corrosion-Damaged Reinforced Concrete Beams.* ACI Structural Journal, 2005. **102**(5): p. 649.
6. Molina, F.J., C. Alonso, and C. Andrade, *Cover cracking as a function of rebar corrosion: Part 2- Numerical model.* Materials and structures, 1993. **26**(9): p. 532-548.
7. Vu, K., G.M. Stewart, and J. Mullard, *Corrosion-Induced Cracking: Experimental Data and Predictive Models.* ACI Structural Journal, 2005. **102**(5): p. 719.
8. Andrade, C., C. Alonso, and F.J. Molina, *Cover cracking as a function of rebar corrosion: Part 1- Experimental test.* Materials and structures, 1993. **26**(9): p. 453-464.
9. Maaddawy, A.E.T. and A.S. Khaled, *Effectiveness of Impressed Current Technique to Simulate Corrosion of Steel Reinforecement in Concrete.* Journal of Material in Civil Engineering 2003. **15**(1): p. 41-47.
10. Amleh, L. and S. Mirza, *Corrosion Influence on Bond between Steel and Concrete.* ACI Structural Journal, 1999. **96**(3): p. 415-423.
11. Law, D., *Residual strength of corrosion damaged structures*. 2005, School of Civil and Chemical Engineering, RMIT,.
12. Cabrera, J.G., *Deterioration of concrete due to reinforcement steel corrosion.* Cement and Concrete Composites, 1996. **18**(1): p. 47-59.
13. Almusallam, A.A., et al., *Effect of reinforcement corrosion on bond strength.* Construction and Building Materials, 1996. **10**(2): p. 123-129.
14. Stanish, K., R.D. Hooton, and S.J. Pantazopoulou, *Corrosion Effects on Bond Strength in Reinforced Concrete.* ACI Materials Journal, 1999. **96**(6): p. 915-921.

15. Mangat, P.S. and M.S. Elgarf, *Bond characteristics of corroding reinforcement in concrete beams.* Materials and Structures, 1999. **32**: p. 89-97.
16. Fang, C., et al., *Bond behaviour of corroded reinforcement steel bars in concrete.* Cement and concrete research, 2006. **36**: p. 1931-1938.
17. Lee, H.-S., T. Noguchi, and F. Tomosawa, *Evaluation of the bond properties between concrete and reinforcement as a function of the degree of reinforcement corrosion.* Cement and Concrete Research, 2002. **32**(8): p. 1313-1318.
18. Malhotra, V.M. and N.J. Carino, *Handbook on Nondestructive Testing of Concrete Chpater 11 Methods to Evaluate Corrosion of Reinforcement*, ed. second. 2004: CRC Press LLC.
19. Annual Book of ASTM standards, *Standard Practice for Calculation of Corrosion Rates and Related Information from Electrochemical Measurements.* 2004.
20. Fang, C., et al., *Corrosion influence on bond in reinforced concrete.* Cement and concrete research, 2004. **34**(11): p. 2156-2167.
21. Gonzalez, J.A., et al., *Comparision of rates of general corrosion and maximum pitting penetration on concrete embedded steel reinforcement.* Cement and concrete research, 1995. **25**(2): p. 257-264.
22. Broomfield, J.P., *Corrosion of steel in Concrete: understanding, investigation, and repair*. 1997: E&FN Spon, Chapman&Hall.
23. Al-Sulaimani, G.J., et al., *Influence of corrosion and cracking on bond behavior and strength of reinforced concrete member.* ACI Structural Journal, 1990. **87**(2): p. 220-231.
24. Rasheeduzzafar, S.S. Al-Saadoun, and Al-Gahtani A.S., *Corrosion Cracking in Relation to Bar Diameter, Cover AND Concrete Quality.* Journal of Materials in Civil Engineering, 1992. **4**(4): p. 327-342.
25. Rodriguez, J., L.M. Ortega, and J. Casal, *Corrosion of reinforcing bars and service life of reinforced concrete structures: Corrosion and bond deterioration*, in *Int. Conference on Concrete across borders,*. 1994: Odense, Denmark,. p. 315-326.
26. Mangat, P.S. and M.S. ELgarf, *Flexural Strength of Concrete Beams with Corroding Reinforcement.* ACI Structural Journal, 1999. **96**(1): p. 149-158.
27. Anyeung, Y., P. Balaguru, and L. Chung, *Bond Behavior of Corroded Reinforcement Bars.* ACI Materials Journal, 2000. **97**(2): p. 214-220.
28. Mohammed, T.U., et al., *Effect of Crack Width and Bar Types on Corrosionof Steel in Concrete.* Journal of Materials in Civil Engineering, 2001. **13**(3): p. 194-201.
29. Francois, R. and G. Arliguie, *Effect of microcracking and cracking on the development*

of corrosion in reinforced concrete members. Magazine of Conrete Research, 1999. **51**(2): p. 143-150.

30. Schieβl, P. and M. Raupach, *Laboratory studies and calculations on the influence of crack width on chloride-induced corrosion of steel in concrete.* ACI Materials Journal, 1997. **94**(1): p. 56-62.
31. Ohtsu, M. and S. Yosimura, *Analysis of crack propagation and crack initiation due to corrosion of reinforcement.* Construction and Building Materials, 1997. **11**: p. 437-442.
32. Andrade, C., et al., *Relation between corrosion and cracking.* Internal report of Brite/Euram Project BE-4062. DG XⅡ, C.E.C, 1995.
33. Tepfers, R., *Cracking of concrete cover along achored deformed reinforcing bars.* Magazine of Conrete Research, 1979. **31**(106).
34. FIB, *Bond of reinforcement in concrete : state-of-art report by Task Group Bond Models*, in *fib bulletin 10*, First, Editor. 2000: Lausane.
35. Wang, X. and X. Liu, *Bond strength modeling for corroded reinforcements.* Construction and Building Materials, 2006. **20**(3): p. 177-186.
36. Bhargava, K., et al., *Corrosion-induced bond strength degradation in reinforced concrete-Analytical and empirical models.* Nuclear Engineering and Design, 2007.
37. Standard, A., *Method 8.1: Method for making and curing concrete- Compression and indirect tesile test specimens*. 2000.
38. AS/NZS, *Steel reinforcing material* 4671:2001.
39. RILEM, -.Ⅱ.-. *RC6 Bond test for reinforcement steel 2. Beam pull-out test*, in *RILEM technical recommendations for the testing and use of construction materials*. 1983. p. 218.
40. Cairns, J. and G.A. Plizzari, *Towards a harmonised European bond test.* Materials and Structures, 2003. **36**: p. 498-506.
41. Chana, P.S., *A test method to establish realistic bond stresses.* Magazine of Concrete Research, 1990. **42**(151): p. 83-90.
42. Rodriguez, J., et al., *Corrosion of reinforcement and service life of concrete structures.* Duability of building materials and components: proceedings of the seventh International Conference, 1996. **1**: p. 117-126.
43. Martin, H. and P. Noakowski, *Bond behavior in reinforced concrete*, r.r. IV, Editor. 1981, Munchen Technical University.
44. Ichinose, T., et al., *Size effect on bond strength of deformed bars.* Construction and

Building Materials, 2004.

45. Baldwin, M.I. and L.A. Clark, *The assessment of reinforcing bars with inadequate anchorage.* Magazine of Conrete Research, 1995. **47**(171): p. 95-102.
46. Soroushian, P., et al., *Bond of Deformed Bars to Concrete: Effects of Confinement and Strength of Concrete.* ACI Materials Journal, 1991. **88**(3): p. 227-232.
47. Abishami, H. and D. Mitchell, *Simulation of uniform of uniform bond stress.* ACI Materials Journal, 1992. **89**(2): p. 161-168.
48. Kayali, O. and S.R. Yeomans, *Bond of ribbed galvanized reinforcing steel in concrete.* Cement and concrete composites, 2000. **22**: p. 459-467.
49. Soylev, T.A. and R. Francois, *Quality of steel-concrete interface and corrosion of reinforcing steel.* Cement and Concrete Research, 2003. **33**(9): p. 1407-1415.
50. Cairns, J., Y. Du, and D. Law, *Influence of corrosion on the friction characteristics of the steel/concrete interface.* Construction and Building Materials, 2005.
51. Okada, K. and T. Miyagawa, *Chloride corrosion of reinforcing steel in cracked concrete, performance of concrete in marine enviroment.* ACI SP-65, 1980: p. 237-254.
52. Liu, Y. and Weyers E. Richard, *Modeling the Time-to-Corrosion Cracking in Chloride Contaminated Reinforced Concrete Structures.* ACI Materials Journal, 1998. **95**(6): p. 675-681.
53. AS3600, *Concrete structure.*
54. Kayyali, O.A. and Y. S.R., *Bond and slip of coated reinforcement in concrete.* Construction and Building Materials, 1995. **9**(4): p. 219-226.

Appendix

Published paper

Tang D.L., Molyneaux T.C.K., Law D., Gravina R. and Ward L. *"The influence of chloride induced corrosion cracks on the strength of reinforced concrete"*, 19th Annual Conference on the Mechanics of Structures and Materials Christchurch, NZ, Dec 2006, Ed. P Moss & R Dhakal, Publ. Taylor & Francis Group, London, UK, ISBN 13-978-0-415-42692-3, Dec 2006

Tang D.L., Molyneaux T.C.K., Law D., and Gravina R. *"Bond strength loss of chloride induced corrosion reinforced concrete specimens"*, SCAMI2 Conference in Changsha, China, Nov. 2007